Estimating the lateral transfer of organic carbon through the European river network using a land surface model

Haicheng Zhang[1*], Ronny Lauerwald[2], Pierre Regnier[1], Philippe Ciais[3], Kristof Van Oost[4], Victoria Naipal[5], Bertrand Guenet[3], Wenping Yuan[6]

[1]Department Geoscience, Environment & Society-BGEOSYS, Université libre de Bruxelles, 1050 Bruxelles, Belgium

[2] Université Paris-Saclay, INRAE, AgroParisTech, UMR ECOSYS, 78850, Thiverval-Grignon, France

[3]Laboratoire des Sciences du Climat et de l'Environnement, IPSL-LSCE CEA/CNRS/UVSQ, Orme des Merisiers, 91191, Gif sur Yvette, France

[4]UCLouvain, TECLIM - Georges Lemaître Centre for Earth and Climate Research, Louvain-la-Neuve, Belgium

[5]EcoAct/ ATOS, 35 rue de miromesnil, 75008, Paris, France

[6]School of Atmospheric Science, Sun Yat-sen University, Guangzhou, Guangdong, 510275, China

Correspondence to: Haicheng Zhang (*haicheng.zhang@ulb.be*)

Formatted: Space After: 18 pt

Abstract. Lateral carbon transport from soils to the ocean through rivers has been acknowledged as a key component of global carbon cycle, but is still neglected in most global land surface models (LSMs). Fluvial transport of dissolved organic carbon (DOC) and CO_2 has been implemented in the ORCHIDEE LSM, while erosion-induced delivery of sediment and particulate organic carbon (POC) from land to river was implemented in another version of the model. Based on these two developments, we take the final step towards the full representation of biospheric carbon transport through the land-river continuum. The newly developed model, called ORCHIDEE-$C_{lateral}$, simulates the complete lateral transport of water, sediment, POC, DOC and CO_2 from land to sea through the river network, the deposition of sediment and POC in the river channel and floodplains, and the decomposition of POC and DOC in transit. We parameterized and evaluated ORCHIDEE-$C_{lateral}$ using observation data in Europe. The model ~~satisfactorily reproduces~~ explains 94%, 75% and 83% of the spatial variations of observed riverine water discharges~~ of water and sediment~~, bankfull water flows and ~~sediment delivery rate from land to river, as well as the observed~~ riverine sediment discharges in Europe, respectively. The simulated long-term average total organic carbon concentrations ~~of organic carbon in~~ and DOC concentrations in river flows are comparable to the observations in major European rivers, although our model generally overestimates the seasonal variation of riverine organic carbon concentrations. Application of ORCHIDEE-$C_{lateral}$ for Europe reveals that the lateral carbon transfer affects land carbon dynamics in multiple ways and omission of this process in LSMs may ~~result in significant biases~~lead to an overestimation of 4.5% in the simulated ~~regional land~~annual net terrestrial carbon ~~budgets~~uptake over Europe. Overall, this study presents a useful tool for simulating large scale lateral carbon transfer and for predicting the feedbacks between lateral carbon transfer and future climate and land use changes.

Formatted: Font: 11 pt

Formatted: Font: 11 pt

1 Introduction

Lateral transfer of organic carbon along the land-river-ocean continuums, involving both spatial redistribution of terrestrial organic carbon and the vertical land-atmosphere carbon exchange, has been acknowledged as a key component of the global carbon cycle (Ciais et al., 2013; Ciais et al., 2021; Drake et al., 2018; Regnier et al., 2013). Erosion of soils and the associated organic carbon, but also leaching of soil dissolved organic carbon (DOC), represent a non-negligible leak in the terrestrial carbon budget and a substantial source of allochthonous organic carbon to inland waters and oceans (Battin et al., 2009; Cole et al., 2007; Raymond et al., 2013; Regnier et al., 2013). As a result of soil aggregate breakdown and desorption, the accelerated mineralization of these eroded and leached soil carbon loads leads to considerable CO_2 emission to the atmosphere (Chappell et al., 2016; Lal, 2003; Van Hemelryck et al., 2011). Meanwhile, the organic carbon that is redeposited and buried in floodplains and lakes might be preserved for a long time, thus creating a CO_2 sink (Stallard, 1998; Van Oost et al., 2007; Wang et al., 2010; Hoffmann, 2022). In addition, lateral redistribution of soil material can alter land-atmosphere CO_2 fluxes indirectly by affecting soil nutrient availability, terrestrial vegetation productivity and physiochemical properties of inland and coastal waters (Beusen et al., 2005; Vigiak et al., 2017).

Although the important role of lateral carbon transfer in the global carbon cycle has been widely recognized, to date, the estimates of land carbon loss to inland waters, the fate of the terrestrial organic carbon within inland waters, as well as the net effect of lateral carbon transfer on land-atmosphere CO_2 fluxes remain largely uncertain (Berhe et al., 2007; Doetterl et al., 2016; Lal, 2003; Stallard, 1998; Wang et al., 2014b; Zhang et al., 2014). Existing estimates of global carbon loss from soils to inland waters vary from 1.1 to 5.1 Pg (=10^{15} g) C per year (yr^{-1}) (Cole et al., 2007; Drake et al., 2018), and the estimated net impact of global lateral carbon redistribution on land-atmosphere carbon budget ranges from an uptake of atmospheric CO_2 by 1 Pg C yr^{-1} to a land CO_2 emission of 1 Pg C yr^{-1} (Lal, 2003; Stallard, 1998; Van Oost et al., 2007; Wang et al., 2017). A reliable model which is able to explicitly simulate the lateral carbon flux along the land-river continuum and also the interactions between these lateral ~~processes~~fluxes and the comprehensive terrestrial carbon cycle, would thus be necessary for ~~predicting~~projecting changes in the global carbon cycle more accurately.

Formatted: English (United States)

Formatted: English (United States)

Formatted: English (United States)

Global land surface models (LSMs) are important tools to simulate the feedbacks between terrestrial carbon cycle, increasing atmospheric CO_2, and climate and land use change. However, the lateral carbon transfer, especially for the particulate organic carbon (POC), is still missing or incompletely represented in existing LSMs (Lauerwald et al., 2017; Lauerwald et al., 2020; Lugato et al., 2016; Naipal et al., 2020; Nakhavali et al., 2021; Tian et al., 2015). It has been hypothesized that the exclusion of lateral carbon transfer in LSMs implies a significant bias in the simulated global land carbon budget (Ciais et al., 2013; Ciais et al., 2021; Janssens et al., 2003). For instance, the study of Nakhavali et al. (2021) suggested that about 15% of the global terrestrial net ecosystem production is exported to inland waters as leached DOC. Lauerwald et al. (2020) showed that the omission of lateral DOC transfer in LSM might lead to significant underestimation (8.6%) of the net uptake of atmospheric carbon in the Amazon basin while terrestrial carbon storage changes in response to the increasing atmospheric CO_2 concentrations were overestimated.

Over the past decade, a number of LSMs ~~has~~have been developed which represent leaching of DOC from soils (Nakhavali et al. 2018, Kicklighter et al. 2013) or the full transport of DOC through the land-river continuum (Lauerwald et al., 2017; Tian et al., 2015). However, the erosion-induced transport of soil POC, which ~~is maybe even more important than~~has also been reported to be able to affect the ~~DOC transport in terms of lateral~~ carbon ~~flux~~balance of terrestrial ecosystems strongly (Lal., 2003; Van Oost et al., 2007; Tian et al., 2015~~; Tan et al., 2017~~), is still not or poorly represented in LSMs. The explicit simulation of the complete transport process of POC at large spatial scales is still a major challenge, due to the complexity of the processes involved, including erosion-induced sediment and POC delivery to rivers, deposition of sediment and POC in river channels and floodplains, re-detachment of the previously deposited sediments and POC, decomposition and transformation of POC in riverine and flooding waters, as well as the changes of soil profile caused by erosion and deposition (Doetterl et al., 2016; Naipal et al., 2020; Zhang et al., 2020).

Several recent model developments have led to the implementation of the lateral transfer of POC in large-scale LSMs. Despite this, there are still some inevitable limitations in these implementations. The Dynamic Land Ecosystem Model (DLEM v2.0, Tian et al., 2015) is able to simulate the erosion-induced POC loss from soil to river and the transport and decomposition of POC in river networks. However, it does not represent the POC deposition in floodplains, nor the impacts of soil erosion and floodplain deposition on the vertical profiles of soil organic carbon (SOC). The Carbon Erosion DYNAMics model (CE-DYNAM, Naipal et al., 2020) simulates erosion of SOC and its re-deposition on the toe-slope or floodplains, transport of POC along river channels, as well as the impact on SOC dynamics at the eroding and deposition sites. However, running at annual time scale, it mostly addresses the centennial timescale and does not represent deposition and decomposition of POC in river channels. Moreover, CE-DYNAM was only applied over the Rhine catchment and has not been fully coupled into a land surface model, therefore excluding the feedbacks of soil erosion on the fully coupled land and aquatic carbon cycles. There are of course more dedicated hydrology and soil erosion models that explicitly simulate the complete transport, deposition and decomposition processes of POC in small river basins (e.g. Jetten et al., 2003; Nearing et al., 1989; Neitsch et al., 2011). However, it is difficult to apply these models at large spatial scales (e.g. continental or global scale) due to the limited availability of forcing data (e.g. geometric attributes of river channel), suitable model parameterization and computational capacity. Moreover, these models have limited capability of representing the full terrestrial C cycle in response to climate change, increasing atmospheric CO_2 and land use change. Therefore, basin-scale models are not an option to assess the impact of soil erosion on the large-scale terrestrial C budget in response to global changes.

Here we describe the development, application and evaluation of a new branch of the ORCHIDEE LSM (Krinner et al., 2005), hereafter ORCHIDEE-$C_{lateral}$, that can be used to simulate the complete lateral transfer processes of water, sediment, POC and DOC along the land-river-ocean continuum at large spatial scale (e.g. continental and global scale). In previous studies, the leaching and fluvial transfer of DOC and the erosion-induced delivery of sediment and POC from upland soil to river network have been implemented in two different branches of the ORCHIDEE LSM (i.e. ORCHILEAK (Lauerwald et al., 2017~~;~~) and ORCHIDEE-MUSLE (Zhang et al., 2020~~).~~)). For this new branch, we first merged these two branches, and subsequently implemented the fluvial transfer of sediment and POC in the coupled model. ORCHIDEE-$C_{lateral}$ is calibrated and evaluated using observation data of runoff, bankfull flow, and riverine loads and concentrations of sediment, POC and DOC across Europe. By applying the calibrated model at European scale, we estimate the magnitude and spatial distribution of the lateral carbon transfer in European catchments during the period 1901-2014, as well as the potential impacts of lateral carbon transfer on the land carbon balance. Comparing simulations results to those of an alternative simulation run with lateral displacement of C deactivated, we finally quantify the biases in simulated land C budgets that arise ignoring the lateral transfers of C along the land-river continuum.

2 Model development and evaluation

2.1 ORCHIDEE land surface model

The ORCHIDEE LSM comprehensively simulates the cycling of energy, water and carbon in terrestrial ecosystems (Krinner et al., 2005). The hydrological processes (e.g. rainfall interception, evapotranspiration and soil water dynamics) and plant photosynthesis in ORCHIDEE are simulated at a time step of 30 minutes. The carbon cycle processes (e.g. maintenance and growth respiration, carbon allocation, litter decomposition, SOC dynamics, plant phenology and mortality) are simulated at daily time step. In its default configuration, ORCHIDEE represents 13 land cover types, with one for bare soil and 12 for lands covered by vegetation ~~by 13 plant functional types (PFTs), with (~~eight ~~PFT for~~types of forests, two ~~for~~types of grasslands, two ~~for~~types of croplands~~, and one for bare soil.~~). Given appropriate land cover maps and parametrization, the number of PFTs to be represented can however be adapted (Zhang et al., 2020).

Our previous implementations of lateral DOC transfer (Lauerwald et al., 2017) and of POC delivery from upland to river network (Zhang et al., 2020) were both based on the ORCHIDEE branch ORCHIDEE-SOM (Camino-Serrano et al., 2018, Fig. S1), which provides a depth-dependent description of the water and carbon dynamics in soil column. In specific, the vertical soil profile in ORCHIDEE-SOM is described by an 11-layer discretization of a 2 m soil column (Camino-Serrano et al., 2018). Water flows between adjacent soil layers are simulated using the Fokker–Planck equation that resolves water diffusion in non-saturated conditions (Campoy et al., 2013; Guimberteau et al., 2018). Free gravitational drainage occurs in the lowest soil layer when actual soil water content is higher than the residual water content (Campoy et al., 2013). Following the CENTURY model (Parton et al., 1988), ORCHIDEE-SOM ~~subdivides the particulate organic carbon stored in soil into~~represents two litter pools (metabolic and structural) and three SOC pools (active, slow and passive) that differ in their respective turnover times. The decomposition of each carbon pool is calculated by first order kinetics based on the corresponding turnover time, soil moisture and temperature as controlling factors, as well as the priming effects of fresh organic matter (Guenet et al., 2018; Guenet et al., 2016). Soil DOC is represented by a labile and a stable DOC pools, with a high and low turnover rate, respectively. Each DOC pool may be in the soil solution or adsorbed on the mineral matrix. The products of litter and SOC decomposition ~~go to~~enter free DOC pool, which in turn is decomposed following first order kinetics (Kalbitz et al., 2003) and returns back to SOC. ~~"The free DOC can then be adsorbed to soil minerals or remain in solution following an equilibrium distribution coefficient (Nodvin et al., 1986), which depends on soil properties (clay and pH). Adsorbed DOC is assumed to be protected and thus is neither decomposed nor transported within the soil column. Free DOC is subject to transport with the water flux between layers calculated by the soil hydrological module of ORCHIDEE, i.e., by advection. Also, SOC and DOC are subject to diffusion that is represented using the second Fick's law of diffusion" (Camino-Serrano et al., 2018, p. 939).~~Adsorption and desorption of DOC follows an equilibrium distribution coefficient calculated from soil clay and pH. Free DOC can be transported with the water flux simulated by the soil hydrological module of ORCHIDEE. However, DOC adsorbed to soil minerals can neither be decomposed nor transported (Camino-Serrano et al., 2018). All the described processes occur within each soil layer. At each time step, "the flux of DOC leaving the soil is calculated by multiplying DOC concentrations in soil solution with the runoff (surface layer) and drainage (bottom layer) flux simulated by the hydrological module" (Camino-Serrano et al., 2018, p. 939). More detailed information about the simulation of soil hydrological and biogeochemical processes in ORCHIDEE-SOM can be found in Guenet et al. (2016) and Camino-Serrano et al. (2018).

2.1.1 Lateral transfer of DOC and CO_2

Lateral transfer of DOC and dissolved CO_2 from land to ocean through river network has been implemented in the ORCHILEAK (Lauerwald et al., 2017), an ORCHIDEE branch developed from ORCHIDEE-SOM (Fig. S1).~~.~~ The adsorption, desorption, production, consumption and transport of DOC within the soil column, as well as DOC export from soil to river along with surface runoff and drainage in ORCHILEAK is simulated using the same method as

ORCHIDEE-SOM. Besides the decomposition of SOC and litter, ORCHILEAK also represents the contribution of wet and dry deposition to soil DOC via throughfall. The direct DOC input from rainfall to aquatic DOC pools is simulated based on the DOC concentration in rainfall and the area fraction of stream and flooding waters in each basin. Simulation of the lateral transfer of DOC and CO_2 in river networks, i.e. the transfer of DOC and CO_2 from one basin to another based on the stream flow directions obtained from a forcing file (0.5°, Table 1), follows the routing scheme of water (Guimberteau et al., 2012). For each basin with floodplain (defined by forcing data), bankfull flow occurs when stream volume in the river channel exceeds a threshold prescribed by the forcing file (Table 1). DOC and CO_2 in flooding waters can enter into soil DOC and CO_2 pools along with the infiltrating water. On the contrary, DOC and CO_2 originated from the decomposition of submerged litter and SOC in the floodplains are added to the overlying flooding waters. Note that the turnover times of litter and SOC under flooding waters are assumed to be three times of the litter and SOC turnover times in upland soil (Reddy & Patrick Jr, 1975; Neckles & Neill, 1994; Lauerwald et al., 2017). After removing the infiltrated and evaporated water, the amount of the remaining flooding water, as well as the DOC and dissolved CO_2 returning to river channel at the end of each day is calculated based on a time constant of flooding water (= 4.0 days, d'Orgeval et al., 2008) modified by a basin-specific topographic index (f_{topo}, unitless) (Lauerwald et al., 2017).

Table 1. List of forcing data needed to run ORCHIDEE-$C_{lateral}$ and the data used to evaluate the simulation results. S_{res} and T_{res} are the spatial and temporal resolution of the forcing data, respectively.

	Data	**S_{res}**	**T_{res}**	**Data source**
Forcing	Climatic forcing data (precipitation, temperature, incoming shortwave/longwave radiation, air pressure, wind speed, relative humidity)	0.5°	3 hour	GSWP3 database (Dirmeyerm et al., 2006)
	Land cover	0.5°	1 year	LUHa.rc2 database (Chini et al., 2014)
	Soil texture class	0.5°	–	Reynolds et al. (1999)
	Soil bulk density and pH	30″	–	HWSD v1.2 (FAO/IIASA/ISRIC/ISSCAS/JRC, 2012)

	Stream flow directions, topographic index (f_{topo})	0.5°	–	STN-30p (Vörösmarty et al., 2000)
	Area fraction of floodplains	250 m	–	GFPLAIN250m (Nardi et al., 2019)[a]
	Area fraction of river surface	0.5°	–	Lauerwald et al. (2015)
	Maximum water storage in river channel (S_{rivmax})	0.5°	–	Derived from pre-runs with ORCHIDEE-$C_{lateral}$ (see section 2.3)
	Reference sediment delivery rate (SED_{ref})	0.5°	–	Zhang et al. (2020)
	Digital Elevation Model (DEM)	3″	–	HydroSHEDS (Lehner et al., 2008) and GDEM v3 (Abrams et al., 2020)[b]
Validation	Riverine water discharge	–	1 day	GRDC[c]
	Bankfull flow	–	1 year	Schneider et al. (2011)
	Sediment delivery from upland to inland waters	100 m	1 year	Borrelli et al. (2018)
	Riverine sediment discharge	–	1 year	European Environment Agency[d] and publications[e]
	Riverine POC and DOC concentration	–	Instantaneous	GLORICH (Hartmann et al., 2019)
		30″		HWSD v1.2
		5′		GSDE (Shangguan et al., 2014)
	SOC stock	250 m	–	SoilGrids (Hengl et al., 2014)
		10 km		S2017 (Sanderman et al., 2017)
		250 m		LandGIS[f]

[a] The GFPLAIN250m only covers the regions south of 60° N. We produced map of floodplain distribution in regions north of the 60° N using the same method for producing GFPLAIN250m (Nardi et al., 2019) based on the ASTER GDEM v3 database (Abrams et al., 2020). [b] The DEM data from HydroSHEDS and GDEM v3 are used to extract the topographic properties (e.g. location, area and average slope) of headwater basins in regions south and north of 60° N, respectively. [c] The Global Runoff Data Centre, 56068 Koblenz, Germany. [d] https://www.eea.europa.eu/data-and-maps/data/sediment-discharges. [e] Publications including Van Dijk & Kwaad, 1998; Vollmer & Goelz, (2006) and Reports of the DanubeSediment project (Sediment Management Measures for the Danube, http://www.interreg-danube.eu/approved-projects/danubesediment). [f] https://zenodo.org/record/2536040#.YC-QGo9KiUm.

~~DOC decomposition and CO_2 evasion in inland waters are simulated using a much fine integration time step of 6 minutes. The decomposition~~Decomposition of DOC in stream and flooding waters is calculated at daily time step based on the prescribed turnover times of labile (2 days) and refractory (80 days) DOC in waters (when temperature is 28 °C) and a temperature factor obtained from Hanson et al. (2011). ~~As described~~CO_2 evasion in ~~Lauerwald et al. (2017), besides CO_2 originated from fluvial DOC, "dissolved CO_2 inputs from the decomposition from flooded SOC and litter are also added at the~~inland waters is simulated using a much fine integration time step of 6 minutes ~~to represent the continuous additions of CO_2 during the water–atmosphere gas exchange. For each time step, the~~. The CO_2 partial pressures (pCO_2) in ~~the~~ water column is first calculated ~~from the concentration of dissolved CO_2 and~~based on the temperature-dependent solubility of CO_2 and the concentration of dissolved CO_2 (Telmer and Veizer, 1999). ~~The~~Then the CO_2 evasion is ~~finally~~ calculated based on the gas exchange velocity, the water–air gradient in pCO_2, ~~the gas exchange velocity~~ and the surface water area available for gas exchange~~" (p. 3835~~ (Lauerwald et al., 2017). In addition, swamp and wetland are also represented in the routing scheme of ORCHILEAK. More detailed descriptions can be found in Lauerwald et al. (2017).

2.1.2 Sediment and particulate organic carbon delivery from upland soil to river network

~~Using~~To give an accurate simulation of sediment delivery from uplands to river network and maintain computational efficiency, an upscaling scheme which integrates information from high-resolution (3″) topographic and soil erodibility data into a LSM forcing file at 0.5° spatial resolution, has been introduced (see details in Zhang et al., 2020, Fig.S2). With this upscaling scheme, the erosion-induced sediment and POC delivery from upland ~~soil~~soils to the river network, as well as the ~~dynamics of vertical~~changes in SOC ~~distribution~~profiles due to soil erosion had already been implemented in ORCHIDEE-MUSLE (Zhang et al., 2020). The sediment delivery from small headwater basins ~~to~~(which are basins without perennial stream and are extracted from high-resolution (e.g. 3″) digital elevation model (DEM) data, Figs. S2a&d) to the river network (i.e. gross upland soil erosion – sediment deposition within headwater basins) is simulated using the Modified Universal Soil Loss Equation model (MUSLE, Williams, 1975). ~~For the upscaling, MUSLE is first applied to high-resolution (3″) topographic and soil erodibility data.~~ As introduced in Zhang et al. (2020), "the daily sediment delivery rate from each headwater basin (S_{i_ref}, Mg day^{-1} basin^{-1}) is first calculated for a given set of reference runoff and vegetation cover conditions~~:~~ (Fig. S2e):

$$~~S_{i_{ref}} = a\left(Q_{i_{ref}} q_{i_{ref}}\right)^{b}~~ \quad S_{i\_ref} = a\left(Q_{i\_ref}\, q_{i\_ref}\right)^{b} K_i LS_i C_{ref} P_{ref} \qquad (1)$$

Formatted: Font color: Auto
Formatted: Font: 11 pt, English (United Kingdom)
Formatted: Font: 11 pt, English (United Kingdom)
Formatted: Font: 11 pt, English (United Kingdom)
Formatted: Font: 11 pt, English (United Kingdom)
Formatted: Font: 11 pt, English (United Kingdom)
Formatted: Font: 11 pt, English (United Kingdom)
Formatted: Font: 11 pt, English (United Kingdom)
Formatted: Font: 11 pt, English (United Kingdom)
Formatted: Font: 11 pt, English (United Kingdom)
Formatted: Font: 11 pt, English (United Kingdom)

where Q_{i_ref} is the total water discharge (m^3 day^{-1}) at the outlet of headwater basin i for the daily reference runoff condition (R_{ref}) of 10 mm day^{-1}. (see Table S1 for the definitions of all abbreviations used in this study). In Eq. 1, q_{i_ref} is the daily peak flow rate (m^3 s^{-1}) at the headwater basin outlet under the assumed reference runoff condition. Similar to the SWAT model (Soil and Water Assessment Tool, Neitsch et al., 2011), q_{i_ref} was calculated from the reference maximum 30-minutes runoff (= 1 mm 30-$minutes^{-1}$) depth and drainage area (DA_i, m^2) according to the following equation:

$$q_{i\_ref} = \frac{R_{30\_ref}}{30 \times 60}\left(DA_i^{(d\,DA_i^{c})}\right)1000 \quad (2)$$

where R_{30_ref} (= 1 mm 30-$minutes^{-1}$) is the assumed daily maximum 30-minutes runoff” (p. 5-6).”. The coefficients a and b in Eq. 1 and c and d in Eq. 2 need to be calibrated (see section 2.3 and Table A12). In Eq. 1, the term LS_i is the combined dimensionless slope length and steepness factor calculated based on the DA_i and the average slope steepness (extracted from DEM) of headwater basin i (Moore and Wilson, 1992). C_{ref} (0-1, dimensionless) in Eq. 1 represents the cover management factor and is set to 0.1 for the reference state. The soil erodibility factor K_i (Mg MJ^{-1} mm^{-1}) is calculated using the method of the EPIC model (Sharpley and Williams, 1990) based on SOC and soil texture data obtained from the GSDE database (Table 1). The term P_{ref} (0-1, dimensionless) in Eq. 1 is a factor representing erosion control practices. It was set to 1, as we did not consider the impacts of soil conservation practices in reducing soil erosion rate. Note that it does not matter which value is chosen for the R_{ref}, R_{30_ref}, C_{ref} and $P_{ref}$$C_{ref}$ as long as they are used consistently throughout a study.

For the use of these reference sediment delivery estimates in ORCHILEAK ORCHIDEE-$C_{lateral}$, the values were first calculated for each headwater basin derived from high resolution geodata, (Fig. S2e), then aggregated to 0.5° grid cells (Fig. S2f) – the scale used in our simulations and required to maintain computational efficiency (also limited by the availability of climate and land cover forcing data).

This aggregated dataset is then used to force the simulation of Then, the actual daily sediment delivery ($S_{iday}$$S_i$, g day^{-1} $grid^{-1}$) in ORCHIDEE Clateralis calculated, by comparing the $C_{lateral}$, simply based on the estimated reference sediment delivery rates of Eq. (1) and on the ratios

Formatted: Subscript

between actual runoff and land cover conditions ~~to~~ and the assumed reference conditions used to create that forcing file (Eq. 4, Fig. S2g).

$$S_{ref} = \sum_{i=1}^{n}(S_{i\_ref}) \times 10^6 \tag{3}$$

~~$$S_{iday} = S_{ref}\left(\frac{R_{iday}\,R_{30\_iday}}{R_{ref}\;R_{30\_ref}}\right)^{b}\frac{C_{iday}}{C_{ref}} \tag{4}$$~~

$$S_j = S_{ref}\left(\frac{R_j\,R_{30\_j}}{R_{ref}\;R_{30\_ref}}\right)^{b}\frac{C_j}{C_{ref}} \tag{4}$$

where ~~R_{iday}~~ R_j (mm day^{-1}) is the ~~daily~~ total surface runoff on day *j* simulated by the hydrological module or ORCHIDEE-MUSLE at 0.5° spatial resolution every 30 minutes. R_{30_j} (mm 30-min^{-1}) is the maximum value of the 48 half-hour runoffs in each day. ~~C_{iday}~~ C_j (0-1, unitless) is the daily actual cover management factor, calculated based on the fraction of surface vegetation cover, the amount of litter carbon and the biomass of living roots in each PFT within each 0.5°×0.5° grid cell. R_{ref}, R_{30_ref}, C_{ref} and P_{ref} are the reference values used to estimate the reference sediment delivery rates as describe above.

Daily POC delivery to river headstream in each 0.5° grid cell is finally simulated based on the sediment delivery rate and the average SOC concentration of surface soil layers (0-20 cm). The vertical SOC profile is updated every day based on the average depth of eroded soil for each PFT in each 0.5° grid cell of ORCHIDEE. For more detailed description of the ORCHIDEE-MUSLE, we refer to Zhang et al. (2020).

2.2 Sediment and POC transport in inland water network

Through the merge of the model branches ORCHILEAK and ORCHIDEE-MUSLE, the new branch ORCHIDEE-$C_{lateral}$ combines the novel features of both sources (DOC and POC) described above. The development of ORCHIDEE-$C_{lateral}$ is complemented by a representation of the sediment and POC transport through the river network that is completely novel and described below.

2.2.1 Sediment transport

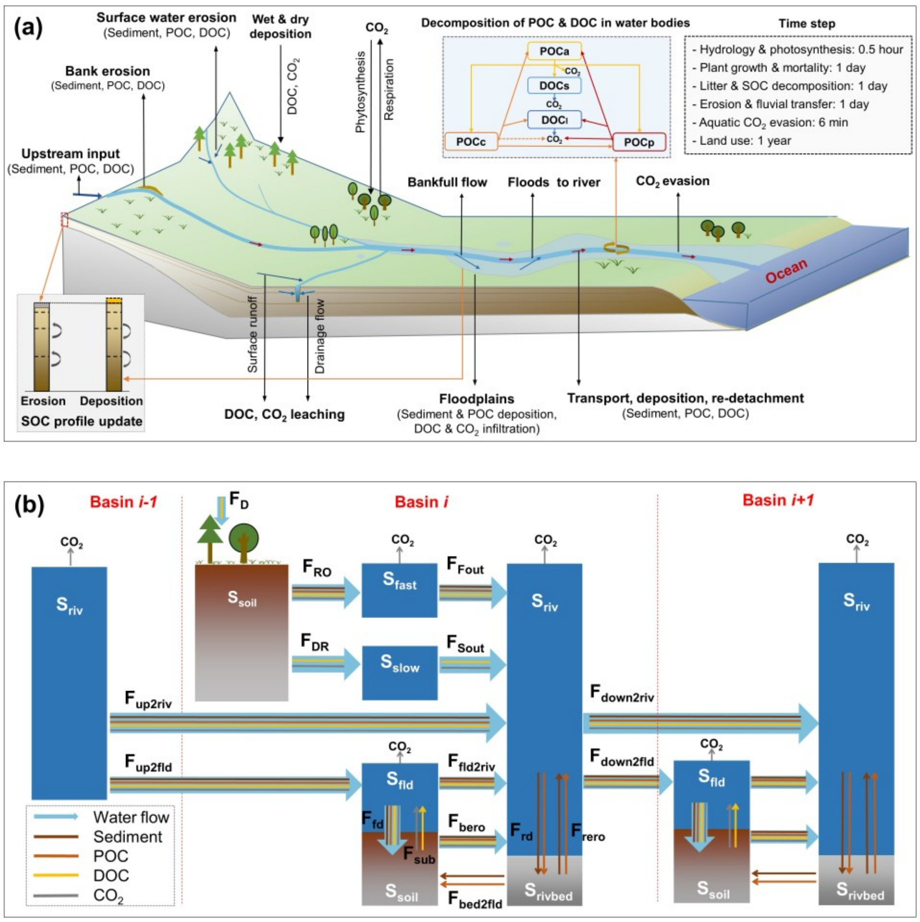

(a)
Surface water erosion
(Sediment, POC, DOC)
Wet & dry deposition
DOC, CO2
CO2
Phytosynthesis
Respiration
Decomposition of POC & DOC in water bodies
POCa
DOCs
DOCl
POCc
POCp
Time step
- Hydrology & photosynthesis: 0.5 hour
- Plant growth & mortality: 1 day
- Litter & SOC decomposition: 1 day
- Erosion & fluvial transfer: 1 day
- Aquatic CO2 evasion: 6 min
- Land use: 1 year
Bank erosion
(Sediment, POC, DOC)
Upstream input
(Sediment, POC, DOC)
Bankfull flow
Floods to river
CO2 evasion
Ocean
Surface runoff
Drainage flow
Erosion
Deposition
SOC profile update
DOC, CO2 leaching
Floodplains
(Sediment & POC deposition, DOC & CO2 infiltration)
Transport, deposition, re-detachment
(Sediment, POC, DOC)
(b)
Basin i-1
Basin i
Basin i+1
FD
CO2
Sriv
Ssoil
FRO
Sfast
FFout
FDR
Sslow
FSout
Fup2riv
Fdown2riv
Fup2fld
Sfld
Ffld2riv
Fdown2fld
Ffd
Fsub
Fbero
Frd
Frero
Fbed2fld
Srivbed
Water flow
Sediment
POC
DOC
CO2

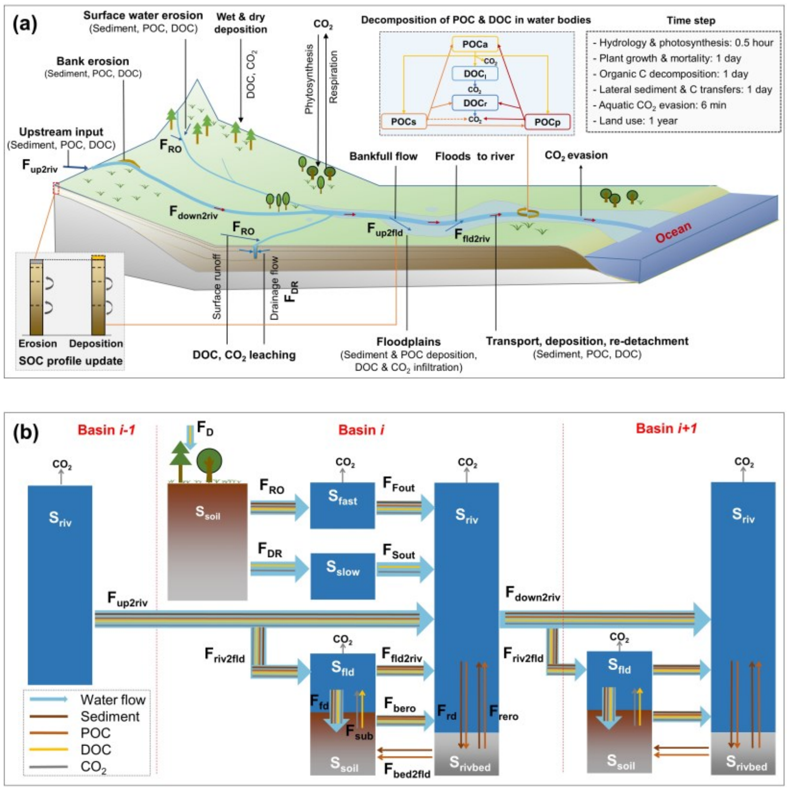

Figure 1 Simulated lateral transfer processes of water, sediment and carbon (POC, DOC and CO_2) in ORCHIDEE-$C_{lateral}$ (a) and a schematic plot for the reservoirs and flows of water, sediment and carbon represented in the routing module of ORCHIDEE-$C_{lateral}$~~.~~ (b). S_{soil} is the soil pool. S_{rivbed} is the sediment (also POC) deposited ~~in~~on the river bed. S_{fast}, S_{slow}, ~~S_{river}~~S_{riv} and ~~S_{flood}~~S_{fld} are the 'fast', 'slow', stream and flooding water reservoir, respectively. F_{RO} and F_{DR} are the surface runoff and belowground drainage, respectively. F_{Fout} and F_{Sout} are the flows from fast and slow reservoir to the stream reservoir, respectively. F_{up2riv} and ~~F_{up2fld}~~$F_{down2riv}$ are the upstream inputs and downstream outputs, respectively. $F_{riv2fld}$ is the outputs from ~~upstream basins to the~~ river stream ~~reservoir and~~ to the flooding reservoir~~ of the target basin, respectively. $F_{dow2riv}$ and $F_{down2fld}$ are the outputs from the stream reservoir of the target basin to the stream reservoir and flooding reservoir of the neighbouring downstream basin, respectively~~. $F_{fld2riv}$ is the return flow from flooding reservoir to stream reservoir. $F_{bed2fld}$ is the transform from deposited sediment in

river bed to floodplain soil. F_{bero} is bank erosion. F_{rd} and F_{rero} are the deposition and re-detachment of sediment and POC in river channel, respectively. F_{sub} is the flux of DOC and CO_2 from floodplain soil (originated from the decomposition of submerged litter and soil carbon) to the overlying flooding water. F_{fd} is the deposition of sediment and POC and the infiltration of water and DOC. F_D is the wet and dry deposition of DOC from atmosphere and plant canopy. DOC_l and DOC_r are the labile and refractory DOC pool, respectively. POC_a, POC_s and POC_p are the active, slow and passive POC pool, respectively.

Formatted: Subscript

Simulation of sediment transport through the river network basically follows the routing scheme of surface water and DOC of ORCHILEAK (Fig. 1). Along with surface runoff (F_{RO_h2o}, m^3 day^{-1}), the sediment delivery (F_{RO_sed}, g day^{-1}) from uplands in each basin (i.e. each 0.5° grid cell in the case of this study) initially feeds an aboveground water reservoir (S_{fast_h2o}, m^3) with a so-called fast water residence time ~~(S_{fast_h2o}, m^3).~~. From this fast water reservoir, a delayed outflow feeds into the so-called stream reservoir (S_{riv}, m^3, Fig. 1b). Daily water (F_{Fout_h2o}, m^3 day^{-1}) and sediment (F_{Fout_sed}, g day^{-1}) flows from fast water reservoir to stream reservoir are calculated from a ~~basin~~grid cell-specific topographic index f_{topo} (unitless, Vörösmarty et al., 2000) extracted from a forcing file (Table 1) and a reservoir-specific factor τ which translates f_{topo} into a water residence time of each reservoir (Eqs. 5, 6). Following Guimberteau et al. (2012), the τ of the fast water reservoir (τ_{fast}) is set to 3.0 days. As the sediment delivery calculated from MUSLE is the net soil loss from headwater basins (gross soil erosion – soil deposition within headwater basins), we assumed that there is no sediment deposition in the fast reservoir, and that all of the sediment in the fast reservoir ~~enter into~~enters the stream reservoir. In addition, only the surface runoff causes soil erosion. The belowground drainage (F_{DR_h2o}, m^3 day^{-1}) only ~~transport~~transports DOC and dissolved CO_2 to the stream reservoir (Fig. 1b).

$$F_{Fout\_h2o} = \frac{S_{fast\_h2o}}{\tau_{fast}\, f_{topo}} \quad (5)$$

$$F_{Fout\_sed} = \frac{S_{fast\_sed}}{\tau_{fast}\, f_{topo}} \quad (6)$$

The budget of the suspended sediment in the stream ~~reservoir~~ (S_{riv_sed}, g) is determined by ~~the~~ ~~F_{Fout}~~F_{out_sed}, the upstream sediment input (F_{up2riv_sed}, g day^{-1}), the sediment input ~~in~~by flooding water returning to the river ($F_{fld2riv\_sed}$, g day^{-1}), the re-detachment of the previously deposited sediment in the river bed (F_{rero_sed}, g day^{-1}), the bank erosion (F_{bero_sed}, g day^{-1}), the sediment deposition in the river bed (F_{rd_sed}, g day^{-1}) and the sediment transported to downstream river stretches ($F_{down2riv\_sed}$, g day^{-1}) and, occasionally, floodplains (~~$F_{down2fld}$~~$F_{riv2fld\_sed}$, g day^{-1}) (Eq. 7).

$$\frac{dS_{riv\_sed}}{dt} = F_{Fout\_sed} + F_{up2riv\_sed} + F_{fld2riv\_sed} + F_{rero\_sed} + F_{bero\_sed} - F_{rd\_sed} - F_{down2riv\_sed} - \sout{F_{down2fld\_sed}} F_{riv2fld\_sed} \quad (7)$$

Sediment transport capacity (TC, g m^{-3}), defined as the maximum load of sediment that a given flow rate can carry, determines the amount of suspended sediment that can be transported to the downstream grid cell (e.g. $F_{down2riv\_sed}$, ~~$F_{down2fld}$~~$F_{riv2fld\_sed}$), as well as the amount of suspended sediment that will deposit on the river bed (F_{rd_sed}) or the erosion rate of the river bed (F_{rero_sed}) or river bank (F_{bero_sed}) (Arnold et al., 1995; Nearing et al., 1989; Neitsch et al., 2011). ~~Several physics-based algorithms have been proposed to accurately calculate the *TC* of stream flows (Arnold et al., 1995; Molinas and Wu, 2001; Nearing et al., 1989). These algorithms mostly require detailed information about the stream power (e.g. flow speed and depth), geomorphic properties of the river channel (e.g. slope and hydraulic radius) and the physical properties of the sediment particles (e.g. median grain size) (Neitsch et al., 2011). They are good predictors to estimate *TC* in rivers with detailed observation data on local stream, soil, geomorphic properties. Unfortunately, it is not practical to implement those algorithms in ORCHIDEE-C$_{lateral}$ due to the lack of appropriate forcing data at large scale as well as the relatively rough representation of stream flow dynamics compared to hydrological models for small basins. For example, runoff and sediment from all headwater basins in one 0.5° grid cell of ORCHIDEE-C$_{lateral}$ are assumed to flow into one single virtual river channel. Although the total river surface area in each grid cell is represented (obtained from forcing file (Table 1), Lauerwald et al., 2015), the length, width and depth of the river channel are unknown. Furthermore, in reality, there can be multiple river channels in the area represented by each grid cell, and these channels might flow to different directions. This illustrates the difficulty to simulate the detailed hydraulic dynamics of the stream flow in each grid.~~

~~We also noticed that previous studies have derived empirical functions of upstream drainage area (e.g. Luo et al., 2017) or upstream runoff (e.g. Yamazaki et al., 2011) to calculate the river width and depth, allowing to simulate the water flow in the river channel using physically-based algorithms. Unfortunately, to obtain a good fit of the simulated river discharges against observations, the parameters in the empirical functions for calculating river width and depth~~

Formatted: Font color: Text 1

~~generally need to be calibrated separately for each catchment (Luo et al., 2017), an approach that is incompatible with large-scale simulations like those performed here. Without such calibration, the simulated geometrical properties of the river channel and runoff are prone to large uncertainties, thus rendering the simulation of sediment transport at continental or global scale using physically-based algorithms a more challenging task.~~

In this study, we used an empirical equation adapted from the WBMsed model, which has been proven effective in simulating the suspended sediment discharges in global large rivers (Cohen et al., 2014), to estimate the TC (g m^{-3}) of stream flow:

$$TC = \frac{\omega\, q_{ave}^{0.3}\, A^{0.5} \left(\frac{q_{iday}}{q_{ave}}\right)^{e_1} (24\times60\times60)}{F_{down2riv\_h2o}} \quad (8)$$

$e_1 = 1.5 - max$ ~~$(0.8, 0.145 \log_{10} A)$~~ $(0.8, 0.145 \log_{10} DA)$

(9)

where ω is the coefficient of proportionality, q_{ave} (m^3 s^{-1}) is long-term average stream flow rate obtained from an historical simulation by ORCHILEAK (Table 1), ~~q_{iday}~~q_j (m^3 s^{-1}) is stream flow rate on day ~~i, A (m^2)~~j, e_1 is an exponent depending on the upstream drainage area~~,~~ (DA, m^2), $F_{down2riv\_}$~~$_{sed}$~~$_{h2o}$ (m^3 day^{-1}) is the daily downstream water discharge from the stream reservoir. In the stream reservoir of each basin, net deposition occurs when TC is smaller than the concentration of suspended sediment, and the daily deposited sediment (F_{rd_sed}, g day^{-1}) is calculated based on the surplus of the suspended sediment:

$$F_{rd\_sed} = c_{rivdep}\left(S_{riv\_sed} - TC\, S_{riv\_h2o}\right) \quad (10)$$

where c_{rivdep} (0-1, unitless) is the daily deposited fraction of the sediment surplus. Net erosion of the previously deposited sediment in river bed (S_{rivbed_sed}, Fig. 1) or the river bank occurs when TC is larger than the concentration of suspended sediment. We assumed that the erosion of river bank occurs only after all of the S_{rivbed_sed} has been eroded. Thus the daily erosion rate (F_{rero_sed}, g day^{-1}) in river channel is calculated as:

$$F_{rero\_sed} = \begin{cases} c_{ebed}\left(TC\, S_{riv\_h2o} - S_{riv\_sed}\right), & c_{ebed}\left(TC\, S_{riv\_h2o} - S_{riv\_sed}\right) \le S_{rivbed\_sed} \\ S_{rivbed\_sed} + c_{ebank}\left(TC\, S_{riv\_h2o} - S_{riv\_sed} - S_{rivbed\_sed}\right), & c_{ebed}\left(TC\, S_{riv\_h2o} - S_{riv\_sed}\right) > S_{rivbed\_sed} \end{cases} \quad (11)$$

where c_{ebed} (0-1, unitless) and c_{ebank} (0-1, unitless) are the fraction of sediment deficit that can be complemented by erosion of river bed and bank, respectively. After updating the S_{riv_sed} based on the F_{rd_sed} or F_{rero_sed}, the sediment discharge to downstream basin ($F_{down2riv\_sed}$, g day^{-1}) is calculated based on the ratio of downstream water discharge to the total stream reservoir:

$$F_{down2riv\_sed} = \left(S_{riv\_sed} - F_{rd\_sed} + F_{rero\_sed}\right)\frac{F_{down2riv\_h2o}}{S_{riv\_sh2o}} \quad (12)$$

In each basin, the bankfull flow occurs when S_{riv_h2o} exceeds the maximum water storage of river channel (S_{rivmax}, g), which is defined by a forcing file (Table 1). Sediment flow from stream to floodplain (~~$F_{down2fld}$~~$F_{riv2fld\_sed}$, g day^{-1}) follows the flooding water, and it is calculated as:

$$\cancel{F_{down2fld\_sed}}F_{riv2fld\_sed} = \left(S_{riv\_sed} - F_{rd\_sed} + F_{rero\_sed}\right)\cancel{\frac{F_{down2fld\_h2o}}{S_{riv\_sh2o}}}\frac{F_{riv2fld\_h2o}}{S_{riv\_sh2o}} \quad (13)$$

$$\cancel{F_{down2fld\_h2o}}F_{riv2fld\_h2o} = \left(S_{riv\_h2o} - F_{down2riv\_h2o} - S_{rivmax}\right)\frac{f_{A\_fld}}{f_{A\_fld}+f_{A\_riv}} \quad (14)$$

where f_{A_fld} (0-1, unitless) and f_{A_riv} (0-1, unitless) is the fraction of floodplain area and river surface area in each basin, respectively. Following the routing scheme of ORCHILEAK, the bankfull flow of a specific basin is assumed to enter the floodplain in the neighbouring downstream basin instead of the basin where it originates.

The sediment balance in flooding reservoir (S_{fld_sed}, g) is controlled by sediment input from the upstream basins (~~F_{up2fld}~~$F_{riv2fld\_sed}$, g day^{-1}), the sediment flowing back to the stream reservoir ($F_{fld2riv\_sed}$, g day^{-1}) and the sediment deposition (F_{fd_sed}, g day^{-1}) (Fig. 1):

$$\frac{dS_{fld\_sed}}{dt} = \cancel{F_{up2fld\_sed}}F_{riv2fld\_sed} - F_{fld2riv\_sed} - F_{fd\_sed} \quad (15)$$

Sediment deposition in ~~flooding water~~floodplain is calculated as the sum of a natural deposition and the deposition due to evaporation (E_{h2o}, m^3 day^{-1}) and infiltration (I_{h2o}, m^3 day^{-1}) of the flooding waters:

$$F_{fd\_sed} = c_{flddep}\, S_{fld\_sed} \cancel{- S_{fld\_sed}} + S_{fld\_sed}\frac{E_{h2o}+I_{h2o}}{S_{fld\_h2o}} \quad (16)$$

where c_{flddep} (0-1, unitless) is the daily deposited fraction of the suspended sediment in flooding waters. After removing the deposited sediment from S_{fld_sed}, $F_{fld2riv\_sed}$ is calculated based on the ratio of ratio of $F_{fld2riv\_h2o}$ to the total flooding reservoir:

$$F_{fld2riv\_sed} = S_{fld\_sed} \frac{F_{fld2riv\_h2o}}{S_{fld\_h2o} - E_{h2o} - I_{h2o}} \quad (17)$$

$$F_{fld2riv\_h2o} = \frac{S_{fld\_h2o} - E_{h2o} - I_{h2o}}{\tau_{flood}\, f_{topo}} \quad (18)$$

where τ_{flood} is a factor which translates f_{topo} (Table 1) into a water residence time of the flooding reservoir. Same to ORCHILEAK, it is set to 1.4 (day m^{-2}) in this study.

Note that as the upland soil in ORCHIDEE is composed of clay, silt and sand particles, so that the dynamics of clay-, silt- and sand-sediment in inland waters are simulated separately. To represent the selective transport of clay-, silt- and sand-sediment, the model parameter ω (Eq. 8) and c_{rivdep} (Eq. 10) are set to different values when calculating the sediment transport capacity and the deposition of surplus suspended sediment for different particle sizes (Table ~~A1).~~ 2). Moreover, as our model mainly aims to simulate the lateral transfer of sediment and carbon at the decadal to centennial timescale, rather than covering the past thousands of years or even longer time periods, we did not consider the evolution and diversion of river channels in our study.

2.2.2 POC transport and decomposition

Many studies described the selective transport of POC and sediment of different ~~particles~~particle sizes. The enrichment ratio (defined as the ratios of fraction of any given component in the transported sediment to that in the eroded soils) of POC in the transported sediment generally showed significant positive correlation to the fine sediment particles (e.g. fine silt and clay), but negative correlation to the coarse sediment particles (Galy et al., 2008; Haregeweyn et al., 2008; Nadeu et al., 2011; Nie et al., 2015). In ORCHIDEE-$C_{lateral}$, the physical movements of POC in inland water systems are simply assumed to follow the flows of finest clay-sediment (Fig. 1b). For example, the fractions of riverine suspended POC which is deposited on the river bed (F_{rd_POC}, g C day^{-1}) or is transported to the river channel ($F_{down2riv\_POC}$, g C day^{-1}) or floodplain

(~~$F_{down2fld}$~~$F_{riv2fld\_POC}$, g C day^{-1}) ~~of the downstream grid cell~~ are assumed to be equal to the corresponding fractions of clay-sediment (Eqs. 19-21). Also flows of suspended POC in flooding waters to floodplain soil (F_{fd_POC}, g C day^{-1}) or back to the stream reservoir ($F_{fld2riv\_POC}$, g C day^{-1}), as well as the resuspension of POC from the river bed (F_{rero_POC}, g C day^{-1}) are scaled to the simulated flows of clay-sediment (Eqs. 22-24). Note that, similar to SOC, the POC in aquatic reservoirs are divided into three pools: the active (POC_a), slow (POC_s) and passive pool (POC_p) (Fig. 1a). The eroded active, slow and passive SOC flow into the corresponding POC pools in the 'fast' water reservoir (Fig. 1b).

$$F_{rd\_POC} = S_{riv\_POC} \frac{F_{rd\_sed\_clay}}{S_{riv\_sed\_clay}} \quad (19)$$

$$F_{down2riv\_POC} = S_{riv\_POC} \frac{F_{down2riv\_sed\_clay}}{S_{riv\_sed\_clay}} \quad (20)$$

~~$F_{down2fld\_POC} = S_{riv\_POC} \frac{F_{down2fld\_sed\_clay}}{S_{riv\_sed\_clay}}$~~

$$F_{riv2fld\_POC} = S_{riv\_POC} \frac{F_{riv2fld\_sed\_clay}}{S_{riv\_sed\_clay}} \quad (21)$$

$$F_{fd\_POC} = S_{fld\_POC} \frac{F_{fd\_sed\_clay}}{S_{fld\_sed\_clay}} \quad (22)$$

$$F_{fld2riv\_POC} = S_{fld\_POC} \frac{F_{fld2riv\_sed\_clay}}{S_{fld\_sed\_clay}} \quad (23)$$

$$F_{bed2fld\_POC} = S_{rivbed\_POC} \frac{F_{bed2fld\_sed}}{S_{rivbed\_sed}} \quad (24)$$

The representation of POC dynamics in the aquatic reservoirs and bed sediment involve as well decomposition, which follows largely the scheme used for SOC (Fig. 1a). However, instead of using the rate modifiers for soil temperature and moisture used in the soil carbon module, daily decomposition rates (F_{POC_i}, g C day^{-1}) of each POC pool (S_{POC_i}, g C) are simulated to vary with water temperature based on the Arrhenius term which is used to simulate the DOC decomposition in ORCHILEAK (Hanson et al., 2011; Lauerwald et al., 2017):

$$F_{POC\_i} = S_{POC\_i} \frac{1.073^{(T_{water}-28.0)}}{\tau_{poc\_i}} \quad (25)$$

where T_{water} (°C) is the temperature of water reservoirs~~.~~ and is calculated from local soil temperature using an empirical function (Lauerwald et al., 2017). For the POC stored in bed sediment, temperature of the stream reservoir is used to calculate the decomposition rate. τ_{POC_i} is the turnover time of the *i* (active, slow and passive) POC pool. We assumed that the base turnover times of active (0.3 year) and slow (1.12 years) POC pools are the same as for the corresponding SOC pools. The passive SOC pool is generally regarded as the SOC which is associated to soil minerals or enclosed in soil aggregates (Parton et al., 1987). During the soil erosion and sediment transport processes, the aggregates break down and the passive POC loses its physical protection from decomposition (Chaplot et al., 2005; Hu and Kuhn, 2016; Polyakov and Lal, 2008; Wang et al., 2014a). To represent the acceleration of passive POC decomposition due to aggregate breakdown, we assume that the turnover time of the passive POC is same to the active POC (0.3 year), rather than the passive SOC (462 years). Similar to the scheme used to simulate SOC decomposition in ORCHILEAK, the decomposed POC from each of the active, slow and passive pool flows to other POC pools, to DOC pools or is released to the atmosphere as CO_2 (Fig. 1). Fractions of the decomposed POC flowing to different POC and DOC pools or to the atmosphere are set to the same values used in ORCHILEAK for simulating the fates of the decomposed SOC pools.

Changes in the vertical SOC profile of floodplain soils following sediment deposition is simulated at the end of every daily modelling time-step, after physical transfers and decomposition of POC have been calculated. The sediment deposited on the floodplain becomes part of the ~~new~~ surface soil layer, and the active, slow and passive POC flow into the active, slow and passive SOC pools in surface soil layer, respectively. SOC in the original surface and subsurface soil layers is transferred sequentially to the adjacent deeper soil layers. As the vertical soil profile in ORCHILEAK is described by an 11-layer discretization of a 2 m soil column, we introduce a deep (> 2 m) soil pool (S_{deep}) to represent the soil and carbon transferred down from the 11th soil layer following ongoing floodplain deposition. Decomposition rates of the organic carbon in this deep soil pool are assumed to be same to those in the 11th (deepest) soil layer. Note that when the soil erosion rate of the floodplain soil is larger than the sediment deposition rate, sediment and organic carbon in S_{deep} move up to replenish the stocks of the 11th soil layer.

2.3 Model application and evaluation

In this study, ~~the~~ ORCHIDEE-$C_{lateral}$ was applied over Europe and parts of Middle East (-30W–70E, 34N-75N, ~~also includes a part of Middle East and Africa,~~ Fig. ~~S1 in the Supplement~~S4), where extensive observation datasets are available to calibrate and evaluate our model (Table 1). The return period of daily bankfull flow ($P_{flooding}$, year), which represents the average interval between two flooding daysevents and is used in this study to produce the forcing file of S_{rivmax} from a pre-run of ORCHILEAK. Note that $P_{flooding}$ is generally shorter than the return period of real flooding events, as the flooding may occur in several continuous days and all the all flooding waters occurring on these continuous days are generally regarded to belong to the same flooding event (supplementary Fig. S3). To our knowledge, existing observational data onS1). $P_{flooding}$ shows substantial spatial variationsare still very limited. Therefore, following climate and topography (Schneider *et al*., . (2011). In this study,), we assumed thatalso use a constant $P_{flooding}$ for allto simulate the bankfull flows from European rivers in Europe are the same and the observed long-term (1961–2000) average bank full flow rate (m^3 s^{-1}) at 66 sites obtained from Schneider *et al*. (2011) was used to calibrate $P_{flooding}$ (=(the optimized value is 0.1 year, Table A1). Same to2). Following Zhang et al. (2020), the parameters *a*, *b*, *c* and *d* in Eq. 1 and 2 (Table A12) were calibrated at 57 European catchments (Fig. S2dS4d) against the modelled sediment delivery data obtained from the European Soil Data Centre (ESDAC, Borrelli et al., 2018). The sediment delivery data from the ESDAC product is simulated by the WaTEM/SEDEM model using high-resolution data of topography, soil erodibility, land cover and rainfall. It has been calibrated and validated using observed sediment fluxes from 24 European catchments (Borrelli et al., 2018).

Parameters controlling sediment transport, deposition and re-detachment (i.e. ω, c_{rivdep}, c_{flddep}, c_{ebed} and c_{ebank}, Table S12) in stream and flooding reservoirs were calibrated against the observed long-term averaged sediment discharge rate (Table 1). We also conducted a sensitivity analysis to test the sensitivity of the simulated riverine sediment and carbon discharges to these parameters, following the method used in Tian et al. (2015). The sensitivity of simulation results was evaluated based on the relative changes in simulated riverine sediment and carbon discharges to a 10% increase and decrease of each parameter (Table S12). Result of the sensitivity analysis shows that the simulated riverine sediment and POC discharges are most sensitive to c_{rivdep} in Eq. 510, followed by ω in Eq. 8 (Fig. S3S5). Compared to c_{rivdep} and ω, the simulated riverine sediment and POC discharges are less sensitive to c_{flddep}, c_{ebed} and c_{ebank}. With 10% changes in c_{flddep}, c_{ebed} or c_{ebank}, the changes in riverine sediment and POC discharges are generally less than 3%. In addition, the changes in simulated riverine DOC and CO_2 discharges are mostly less than 1% with 10% changes in ω, c_{flddep}, c_{ebed} and c_{ebank}. Nonetheless, a 10% change in c_{rivdep} can lead to a change of about 5% in the simulated riverine CO_2 discharge (Fig. S3).S5).

Table 2 Values of the key parameters used in the ORCHIDEE-$C_{lateral}$ to simulate the lateral transfer of sediment and carbon.

Parameter	**Value**	**Unit**	**Description**	**Source**
a	26.96	Unitless	Coefficient in Eq. 1	Calibrated
b	0.76	Unitless	Coefficient in Eq. 1	Calibrated
c	1.79	Unitless	Coefficient in Eq. 2	Calibrated
d	-0.065	Unitless	Coefficient in Eq. 2	Calibrated
c_{ebed}	0.5	Unitless (0-1)	The fraction of sediment deficit that can be complemented by erosion of river bed (Eq. 6)	Calibrated
c_{ebank}	0.5	Unitless (0-1)	The fraction of sediment deficit that can be complemented by erosion of river bank (Eq. 6)	Calibrated
c_{rivdep}	0.1, 0.2, 0.5[a]	Unitless (0-1)	Daily deposited fraction of the sediment surplus in stream reservoir (Eq. 5)	Calibrated
c_{flddep}	0.5, 1.0, 1.0[a]	Unitless (0-1)	Daily deposited fraction of the sediment surplus in flooding reservoir (Eq. 11)	Calibrated
$P_{flooding}$	0.1	year	Return period of daily bankfull flow	Calibrated
τ_{fast}	3.0	day	A factor which translates the topographic index into the water residence time of the 'fast' reservoir (Eqs. 5, 6)	Guimberteau et al., 2012
τ_{flood}	1.4	day	A factor which translates the topographic index into the water residence time of the flooding reservoir (Eq. 18)	Guimberteau et al., 2012
τ_{poc}	0.3, 1.12, 0.3[b]	year	A factor which translates the topographic index into the water residence time of the flooding reservoir (Eq. 25)	Lauerwald et al., 2017
ω	12.0, 5.0, 2.5[a]	$g\ s^{-1}$	Coefficient of proportionality for calculating sediment transport capacity (Eq. 8)	Calibrated

[a] For clay, silt and sand sediment, respectively. [b] For active, slow and passive POC, respectively.

Formatted: English (United Kingdom)

After parameter calibration, ORCHIDEE-$C_{lateral}$ was applied to simulate the lateral transfers of water, sediment and organic carbon in European rivers over the period 1901-2014. Before this historical simulation, ORCHIDEE-$C_{lateral}$ was run over 10,000 years (spin-up) until the soil carbon pools reached a steady state. In the 'spin-up' simulation, the PFT maps, atmospheric CO_2 concentrations and meteorological data during 1901–1910 were used repeatedly as ~~the~~ forcing data. The finally simulated water discharge rates in European rivers were evaluated using observation data at 93 gauging sites (locations see Fig. ~~S2a~~S4a) from the Global Runoff Data Base (GRDC, Table 1). The simulated bankfull flows were evaluated against observed long-term (1961–2000) average bankfull flows at 66 sites (Fig. ~~S2b~~S4b) from Schneider *et al*. (2011). The simulated riverine sediment discharge rate is evaluated using observation data from the European Environment Agency and existing publications (see Table 1) at 221 gauging sites (Fig. ~~S2c~~S4c). The riverine total organic carbon (TOC), POC and DOC concentrations provided by the GLObal RIver Chemistry Database (GLORICH, Hartmann et al., 2019) at 346 sites (Fig. ~~S2d~~S4d) were used to evaluate the simulated riverine POC and DOC concentrations. Note that observations in the GLORICH database which are measured at gauging sites with drainage area $<1.0\times10^4$ km^2 were excluded from our model evaluation, because these small catchments cannot be represented by the coarse river network scheme at 0.5 degree (ca. 55 km at the equator). Among the retained 346 gauging sites, TOC concentrations were measured at 188 sites, DOC was measured at 314 sites. POC was measured at only ~~3~~two sites (Bad honnef (51 measurements) and Bimmen (78 measurements)) in the Rhine catchment~~.~~ and one site (Rheine, 36 measurements) in the Ems catchment (Fig. S4d).

3 Results and Discussion

3.1 Model evaluation

3.1.1 Stream water discharge and bankfull flow

Evaluation of our simulation results using *in situ* observation data from Europe rivers indicates that ORCHIDEE-$C_{lateral}$ well reproduces the magnitude and interannual variation of water discharge rates in major European rivers (Figs. 2a and ~~S4~~S6). Overall, the simulated riverine water discharge rate explained 94% (Fig. 2a) of the spatial variation of the observed long-term average water discharge rates across 93 gauging sites in Europe (Fig. ~~S2a~~S4a). Relative biases (calculated as: $\frac{simulation-observation}{observation} \times 100\%$, as used through the manuscript if not otherwise stated) of the simulated average water discharge rates compared to the observations are mostly smaller than 30% (Fig. 2a). For major European rivers, such as the Rhine, Danube, Elbe, Rhone and Volga, ORCHIDEE-$C_{lateral}$ also captures the interannual variation of the water discharge rate (Fig. S4S6). We recognize that ORCHIDEE-$C_{lateral}$ may overestimate or underestimate the water discharge rate in some rivers (Fig. 2a), particularly in smaller rivers where discrepancy between the stream routing scheme (delineation of catchment boundaries) extracted from the forcing data at 0.5° resolution and the real river network (Fig. S5S7) can be substantial. An over-estimation or underestimation of the catchment area by the forcing data as respectively found for the Elbe and Rhine will introduce a proportional bias toin the average amount of simulated discharge from thatthese catchment. Another problem are stream channel bifurcations which occur in reality, but which are not represented in a stream network derived from a digital elevation model. For example, in the Danube river delta, a fraction of the discharge is actually exported to the sea through the Saint George Branch, in addition to the water discharge through the main river channel (Fig. S5bS7b). This explains why the simulated water discharge rate at the outlet of the Danube catchment is larger than the observation at the Ceatal gauging station, Romania (identify number in the GRDC database is 6742900, Fig. S4mS6m), where only the main stream discharge was measured.

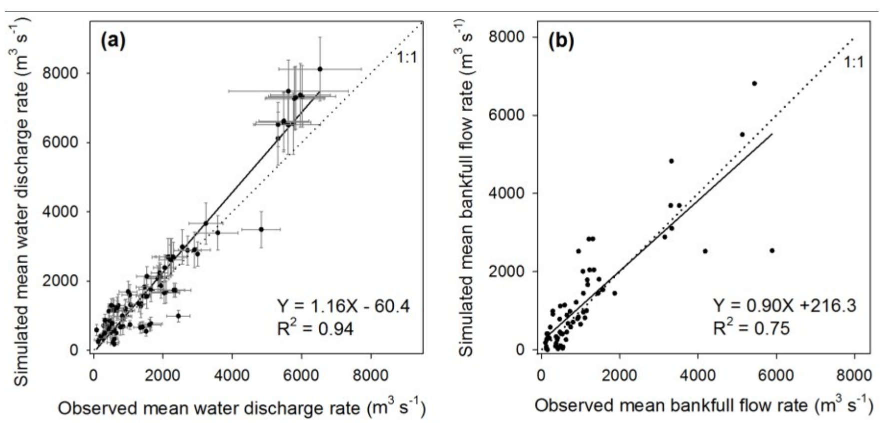

Figure 2 Comparison between observed and simulated riverine water discharge rates (a) and bankfull flow rates (b). In figure (a), the error bar denotes the standard deviation of interannual

variation. Sources of the observed riverine water discharge rate and bankfull flow rate can be found in Table 1.

~~By setting~~With the calibrated return period (= 0.1 year) of the daily flooding rate ~~to 0.1 year,~~(see section 2.3), the simulated bankfull flow rates compare well to observations at the 66 sites for which data was available (Fig. 2b). Overall, the simulation result explained 75% of the inter-site variation of the observed bankfull flow rates. Relative biases of the simulated bankfull flow rates are generally lower than 30%, although the relative bias may be larger than 100% at some sites.

3.1.2 Sediment transport

The simulated area-averaged sediment delivery rates from upland to river network by the ORCHIDEE-$C_{lateral}$ are overall comparable to those simulated by the WaTEM/SEDEM for most catchments in Europe (Figs. 3a and ~~S2d~~S4d). In the two catchments in the Apennine Peninsula, ORCHIDEE-$C_{lateral}$ gives a drastically lower estimation on the sediment delivery rates compared to WaTEM/SEDEM. By excluding these two catchments, ORCHIDEE-$C_{lateral}$ reproduces 72% of the spatial variation of the sediment delivery rates estimated by the WaTEM/SEDEM (Fig. 3a). In addition, the average sediment loss rate over all catchments showed in Fig. S4d is 40.8 g m^{-2} yr^{-1}, which is overall comparable to the estimate by the WaTEM/SEDEM (42.5 g m^{-2} yr^{-1}).

ORCHIDEE-$C_{lateral}$ reproduces 83% of the inter-site variation of the sediment discharge rates across Europe (Fig. 3b). Simulation of the riverine sediment discharge rate at large spatial scale is still a big challenge. It generally needs detailed information on the stream flow, geomorphic properties of river channel and the particle composition of the suspended sediment (Neitsch et al., 2011). Moreover, the parameters of existing sediment transport models usually require recalibration when they are applied to different catchments (Gassman et al., 2014; Oeurng et al., 2011; Vigiak et al., 2017). In ORCHIDEE-$C_{lateral}$, the sediment processes in river networks are simulated using simple empirical functions and parameters based on a routing scheme at a spatial resolution of 0.5° (section 2.2.1). Detailed information about the stream flow (e.g. cross-sectional area) and the geomorphic properties of river channels are not represented. Sediment discharge in all catchments was simulated using a universal parameter set. This may explain why

ORCHIDEE-$C_{lateral}$ fails to capture the sediment discharge rates in some specific catchments, especially those with relatively small drainage areas (e.g. < 5×10^3 km^2).

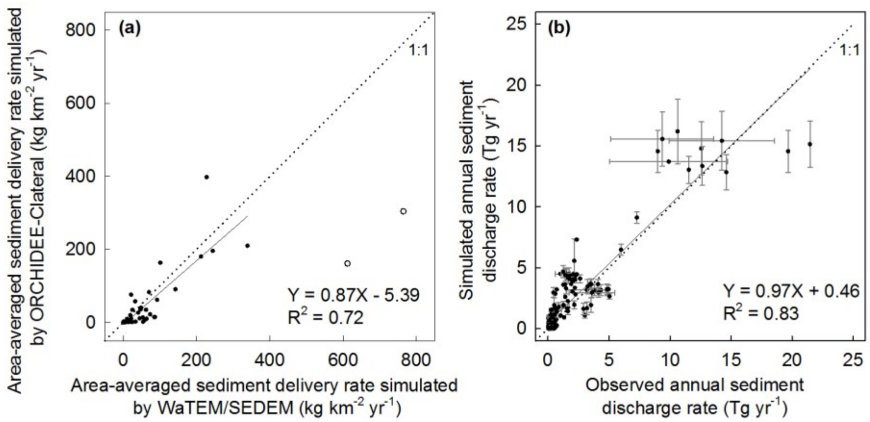

Figure 3 Comparison between the simulated area-averaged sediment delivery rate from uplands to river network from ORCHIDEE-$C_{lateral}$ and WaTEM/SEDEM (a), and the comparison between observed and simulated annual sediment discharge rates at 221 gauging sites (b). In figure (a), the two hollow dots represent the sediment delivery rates at the two catchments in the Apennine Peninsula (Fig. ~~S1d~~S4d). The regression function in figure (a) was obtained based on the values of all solid dots, excluding the two hollow dots. In figure (b), the error bar denotes the standard deviation of interannual variation. Sources of the observed annual sediment discharge rate in Table 1.

3.1.3 Organic carbon transport

Simulation of the riverine carbon discharge rate at large spatial scale is even a bigger challenge than simulating sediment discharge, as the riverine carbon discharge is controlled by many factors, such as upland topsoil SOC concentrations, soil erosion rate, transport and deposition rate of clay fraction in river channel and on floodplain, and the decomposition of POC in transit and in aquatic sediments. As described above, the simulated water discharge rate, bankfull flow and sediment discharge rate are overall comparable to observation (Figs. 2 and 3). The simulated total SOC stock in the top 0-30 cm soil layer in Europe of 107 Pg C is close to the value extracted from the HWSD database (106 Pg C), but significantly lower than the values extracted from some other databases, such as the GSDE (249 Pg C), SoilGrids (202 Pg C), S2017 (148 Pg C) and landGIS (226 Pg C) (Fig. S6aS8a). Distribution of the simulated SOC stock along the latitude gradients (30° N – 75° N) are overall comparable to those extracted from the HWSD and S2017 databases (Fig. S6S8). But even compared to these two databases, our model still underestimated the SOC stock in southern Europe (30° N – 41° N).

Comparison of the simulated concentrations of riverine organic carbon and the observations obtained from the GLORICH database (Hartmann et al., 2019) indicates that our model can basically capture the TOC and DOC concentrations in European rivers (Figs 4, 5, S7S9 and S8S10). The simulation results explain 34% and 32% of the inter-site variation of the observed TOC and DOC concentrations, respectively (Fig. 4). For major European rivers, such as the Rhine, Elbe, Danube, Spree and Weser, the simulated long-term average TOC and DOC concentrations are overall close to the observations (FigFigs. 5, S7S9 and S8S10). But for the Rhone river in southern France, the DOC concentrations have been systematically overestimated by more than 50% (FigFigs. 5 and S8mS10m). In addition, both simulated and observed TOC and DOC concentrations show drastic temporal (both seasonal and interannual) variations (Figs 4, S7S9 and S8S10). Our model seems to have overestimated the temporal variation of TOC and especially DOC concentrations (Figs S7 and S8). . S9 and S10). Nonetheless, the simulated temporal variation of TOC and DOC discharge rates are overall comparable to the observation (Figs. S11 and S12), as our model can well capture the magnitude and temporal variation of riverine water discharge rates.

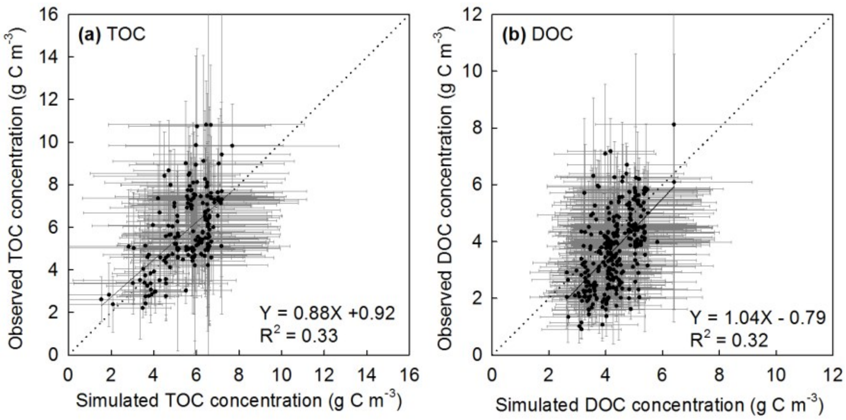

Figure 4 Comparison between the observed and simulated riverine TOC (a, POC+DOC) and DOC (b) concentrations. The dot and error bar denote the mean and standard deviation at each gauging site, respectively. ~~Not~~Note that the mean and standard deviation of the simulated concentrations at each site are calculated based on the monthly average value, but the mean and standard deviation of the observed concentrations are based on instantaneous observation.

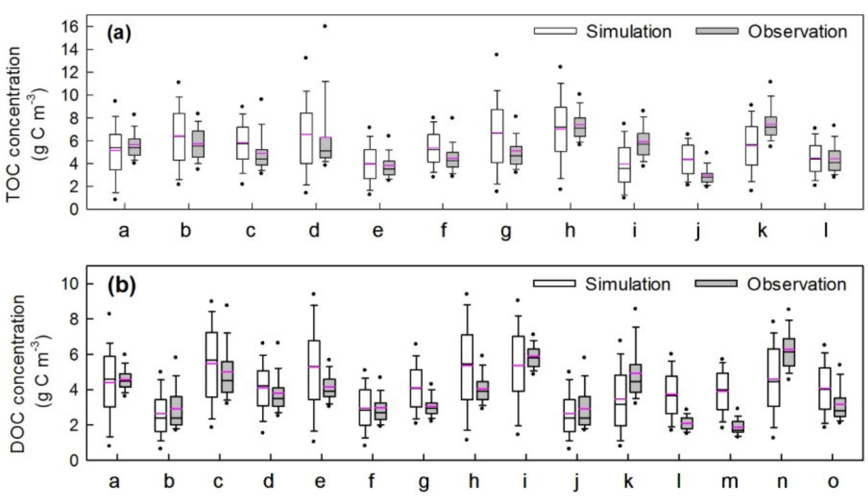

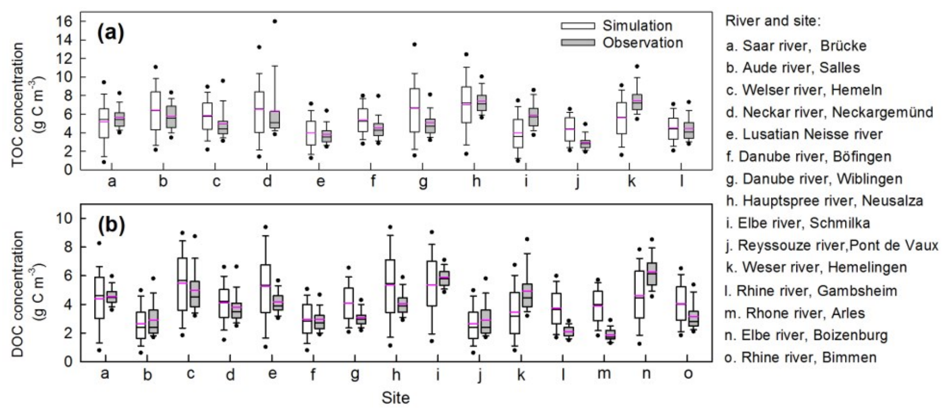

Figure 5 Comparison between the observed and simulated concentrations of total organic carbon (TOC, a) and dissolved organic carbon (DOC, b) in river flows. The black and pink lines in each box denote the median and mean value, respectively. Box boundaries show the 25th and 75th percentiles, whiskers denote the 10th and 90th percentiles, the dots below and above each box denote the 5th and 95th percentiles, respectively.~~ The specific gauging station represented by a-o in figure (a) and (b) can be found in the corresponding sub-plot in Figure S7 and S8, respectively.~~

In Europe, the GLORICH database only provides POC concentrations measured at three gauging stations in northwestern Germany (Figs. 6, ~~S2d~~S4d). The simulated POC concentrations and discharge rates in the Ems river at Rheine are overall comparable to the observation (~~Fig~~Figs. 6e, f). However, at the two gauging sites at the river Rhine, the POC concentrations have been significantly underestimated (Figs. 6a-d). We noticed that the stream routing scheme of Rhine catchment at 0.5° obtained from the forcing data STN-30p (Vörösmarty et al., 2000) differs significantly from the stream routing scheme extracted based on high resolution (3″) DEM~~.~~ (Fig. S7). Thus, besides the errors in simulated SOC stocks, soil erosion rate, stream discharge rate, and sediment transport and deposition rate, the inaccurate stream routing scheme used in this study might also be an important reason for the underestimation of POC concentration in Rhine river.

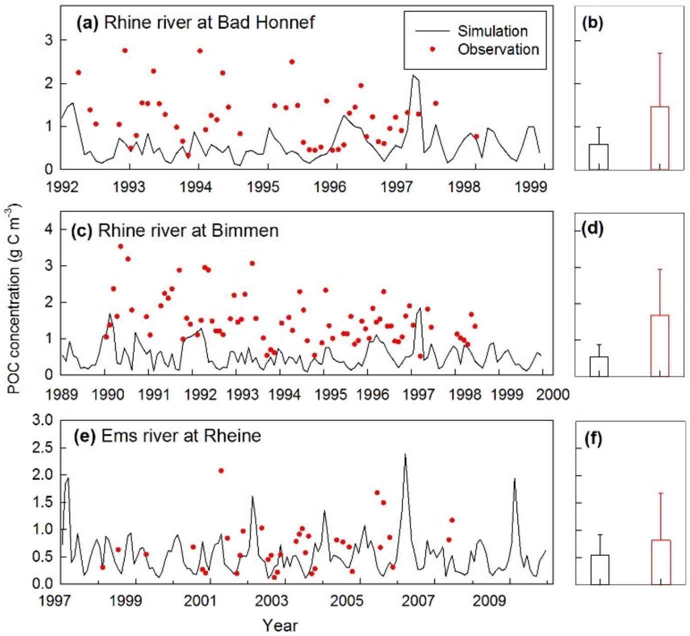
(a) Rhine river at Bad Honnef
Simulation
Observation
(b)
(c) Rhine river at Bimmen
(d)
(e) Ems river at Rheine
(f)
POC concentration (g C m-3)
Year

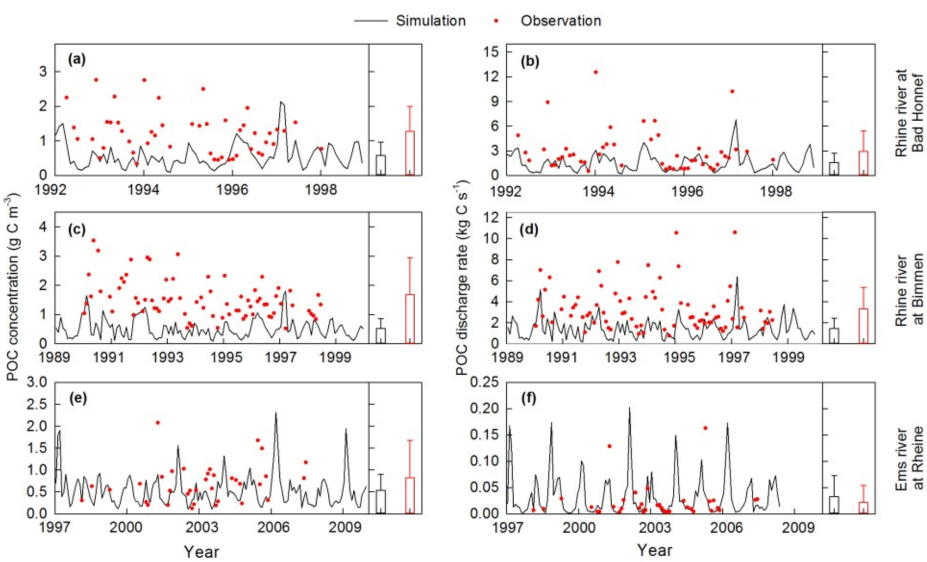
Simulation
Observation
(a)
(b)
(c)
(d)
(e)
(f)
POC concentration (g C m-3)
POC discharge rate (kg C s-1)
Rhine river at Bad Honnef
Rhine river at Bimmen
Ems river at Rheine
Year

Figure 6 Comparison between ~~the~~ observed (instantaneous ~~measurement~~measurements) and simulated (monthly average ~~value~~values) riverine POC concentrations and POC discharge rates at three gauging sites. ~~In figure (b), (d) and (f), the histogram~~The histograms and error ~~bar~~bars denote the ~~mean~~means and standard ~~deviation~~deviations of POC concentrations, respectively. Long-term average water discharge rates at Bad Honnef, Bimmen and Rheine during the observation periods are 2023, 2100 and 80 $m^3 s^{-1}$, respectively.

3.2 Lateral carbon transfers in Europe

Based on our simulation results, the average annual sediment delivery from upland to the river network caused by water erosion in Europe (-30W– 70E, 34N-75N) during 1901-2014 is 2.8±0.4 Pg yr^{-1} (Fig. 7a). From Northern to Southern Europe, the sediment delivery rate from upland to river increase from less than 1.0 g m^{-2} yr^{-1} in the Scandinavia Peninsula, which is covered by mature boreal forests (Fig. ~~S9a~~S13a), and in the Northern European Plain to more than 600 g m^{-2} yr^{-1} in the mountainous regions of the Apennine Peninsula, Balkan Peninsula and the Middle East (Figs. 8a, ~~S10a~~S14a). The Caucasus is mainly covered by ice and bare rock (Fig. ~~S9~~S13), thus the sediment delivery rate in this region is also very low. In total across Europe, ~~55~~63.2% (1.8±0.2 Pg yr^{-1}) of the sediment delivered into river network is deposited in river channels and floodplains, and the remaining 36.8% (1.0±0.1 Pg yr^{-1}) is exported to the sea (Fig. 7a). Generally, large rivers, like Danube, Volga, and Ob rivers, carry more sediment to the sea than small rivers (Figs. 8b, c). But several relatively small rivers in the Middle East and the Po river in northern Italy also carry similarly large amount of sediment to the sea, as the upland soil erosion rates are very high (> 200 g m^{-2} yr^{-1}) in these catchments (Figs. 8a, c). Spatial distribution of the sediment deposition is controlled by the stream routing scheme and the spatial distribution of floodplains (Fig. 9b). In Northern and Central Europe, the area-averaged sediment deposition rates (i.e. amount of annual sediment deposition /area of 0.5°×0.5° grid cell) in river channels and floodplains are mostly less than 100.0 g m^{-2} yr^{-1} (Fig. 8d). In the downstream part of the Danube, Po and several rivers in the Middle East, the sediment deposition rate can exceed 800.0 g m^{-2} yr^{-1}. From 1901 to 1960s, the annual total sediment delivery from uplands to the whole river network of Europe declined significantly (p<0.01, independent sample t-test) from about 3.0 Pg yr^{-1} to about 2.3 Pg yr^{-1} (Fig. S11aS15a). From 1960 to 2014, the annual sediment delivery rate did not show a significant trend, but revealed large interannual variations.

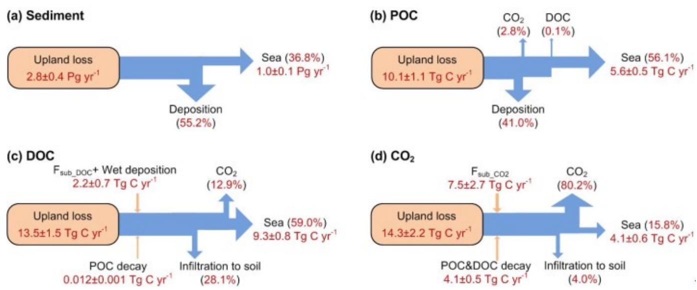

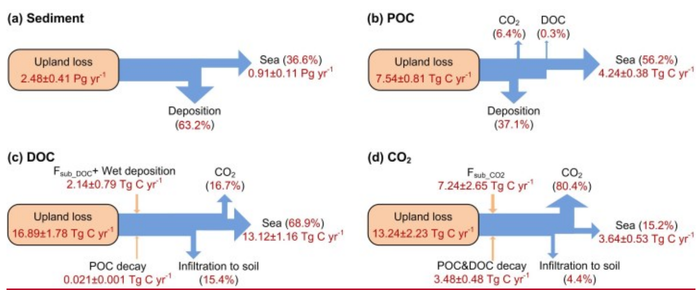

Figure 7 Averaged annual lateral redistribution rate of sediment (a), POC (b), DOC (c) and CO_2 (d) in Europe for the period 1901-2014. F_{sub_DOC} and F_{sub_CO2} are the DOC and CO_2 inputs from floodplain soil (originated from the decomposition of submerged litter and soil carbon) to the overlying flooding water, respectively.

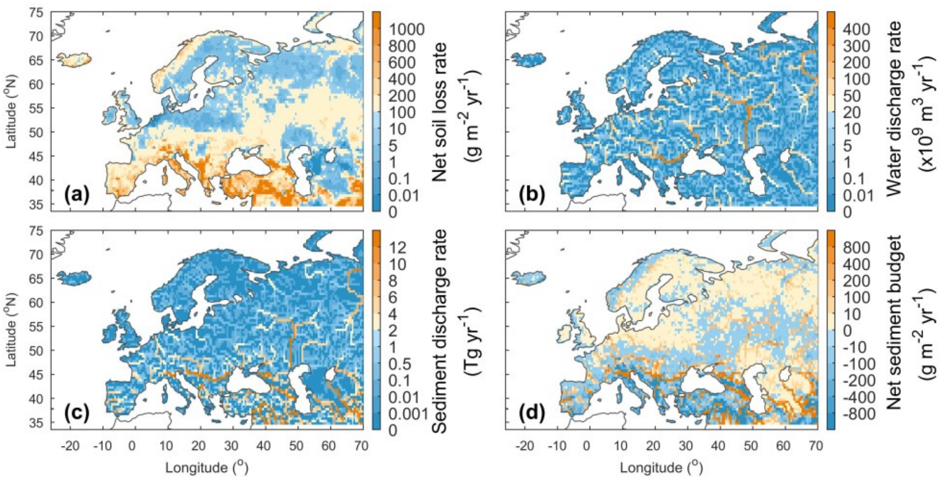

Figure 8 Averaged annual lateral redistribution rate of water and sediment in Europe during 1901-2014. (a) Annual sediment delivery rate from upland to river network; (b) annual water discharge rate; (c) annual sediment discharge rate and (d) annual net sediment budget in each 0.5°×0.5° grid cell. In figure d, the positive and negative values denote net gain and net loss of sediment, respectively.

Along with soil erosion and sediment transport, the average annual POC delivery from upland to river network in the whole Europe during 1901-2014 is 10.1±1.1 Tg C yr^{-1} (Fig. 7b). 41.0% of the POC delivered into the river network is deposited in river channels and floodplains, 2.9% is decomposed during transport, and the remaining 56.1% is exported to the sea. Spatial patterns of the area-averaged SOC delivery rate and POC discharge rate basically follow that of sediment (Fig. 9a, c). ~~But although~~Although the sediment discharge rates in some~~ small~~ rivers in the Middle East can be as high as that in the Danube or Volga river (Fig. 8c), the POC delivery rates in these ~~small~~ rivers ~~is~~are much smaller than in the larger ones (Fig. 9c). This is mainly due to the lower SOC stocks in the Middle East compared to those found in the Danube and Volga catchments (Fig. ~~S6~~S8). We also note that different from the sediment delivery, the annual total POC delivery from upland to river network in Europe did not show a significant declining trend from 1901 to 1960s (Fig. ~~S11b~~S15b). The increase in SOC stock (Fig. ~~S11c~~S15c) may have partially offset the decline in sediment delivery rate.

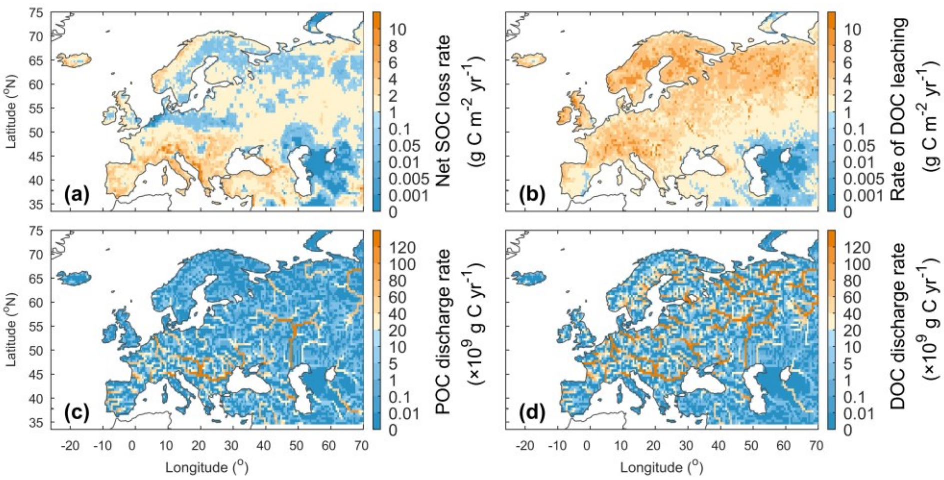

Figure 9 Averaged annual lateral redistribution rate of organic carbon in Europe during 1901-2014. (a) Annual SOC delivery rate from upland to river network; (b) annual DOC leaching rate; (c) annual POC discharge rate and (d) annual DOC discharge rate.

Leaching results in an average annual DOC input of 13.5±1.5 Tg C yr^{-1} from soil to the river network in Europe, and the *in-situ* DOC production caused by wet deposition and the decomposition of riverine POC and submerged litter and soil organic carbon under flooding waters amounts to 2.2±0.7 Tg C yr^{-1} (Fig. 7c). 28.1% of the total riverine DOC is then infiltrating into the floodplain soils, 12.9% is decomposed during riverine transport, and the remaining 59.0% is exported to the sea. The spatial distribution of the DOC leaching rate is very different from that of POC (Fig. 9b). From North-western Europe to Southeast Europe and the Middle East, the DOC leaching rates decrease from over 6 g C m^{-2} yr^{-1} to less than 1.0 g C m^{-2} yr^{-1}. DOC discharge rates in major European rivers, such as Rhine, Danube, Volga, Elbe and Ob, are mostly higher than 100 Tg C yr^{-1} (Fig. 9d). Comparatively, the DOC discharge rates in Southern Europe and the Middle East are significantly lower (<60 Tg C yr^{-1}).

The average annual leaching rate of CO_2 sourced from the decomposition of upland litter and soil organic carbon (incl. DOC) in the whole Europe is 14.3±2.2 Tg C yr^{-1} (Fig. 7a). Decomposition of the submerged litter and organic carbon in floodplains and the decomposition of riverine POC and DOC add an an *in-situ* CO_2 production amounting to 7.5±2.7 Tg C yr^{-1} and 4.1±0.5 Tg C yr^{-1}, respectively. Most of this CO_2 (80.2%) feeding stream waters is then released back to the atmosphere quickly, in such a way that only 15.8% of the CO_2 is exported to the sea, and 4.0% is infiltrated into the floodplain soils.

3.3 Implications for the terrestrial C budget of Europe

Representing the lateral carbon transport in LSM is helpful to estimate the terrestrial carbon cycle more accurately. From the year 1901 to 2014, soil erosion and leaching combined resulted in a 5.4 Pg loss of terrestrial carbon to the European river network, this amount corresponding to about 5% of the total SOC stock (106 Pg C, Fig. ~~S6a~~S8a) in the 0-30 cm soil layer. The average annual total delivery of organic carbon (POC+DOC) during the same period is 47.3±6.6 Tg C yr^{-1} (Fig. 7), which is about 4.7% of the net ecosystem ~~exchange (NEE~~production (NEP (993±255 Tg C yr^{-1}), defined as the difference between the vegetation primary production (NPP) and the soil heterotrophic respiration (Rh) due to the decomposition of litter and soil organic matter~~(~~, i.e. ~~NEE~~NEP=NPP–Rh~~)),~~), and 19.2% of the net biome production (NBP (243±189 Tg C yr^{-1}), defined as the difference between NEP and the land carbon loss (Rd) due to the additional disturbances (e.g. harvest, land cover change, and soil erosion and leaching, i.e. NBP=NEP–Rd–DOC and POC to river) (Fig. 10b). The annual total export of carbon to the sea surrounding Europe is 19.0±1.4 Tg C yr^{-1}, which amounts to 1.9% and 8.7% of the NEE and NBP, respectively.

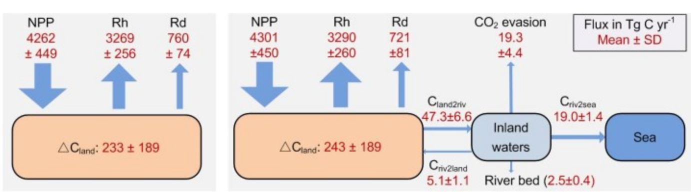

(a) No lateral C transport **(b)** With lateral C transport

Figure 10 The simulated average annual carbon budget of the terrestrial ecosystem in Europe during the 1901-2014 when the lateral carbon transport is ignored (a) and considered (b). All fluxes are presented as mean ± standard deviation. NPP is the net primary production. Rh and Rd are the heterotrophic respiration and the respiration due to disturbances like harvest and land cover change, respectively. ΔC_{land} is the average annual changes of the total land carbon stock.

Percentage following each of these changes in blue is the average annual relative changes of the corresponding carbon pool. $C_{land2riv}$, $C_{riv2land}$ and $C_{riv2sea}$ are the average annual carbon fluxes from land to inland waters, from inland waters to ~~river~~floodplains and from inland waters to the sea, respectively. SD is the standard deviation.

Besides direct transfers of organic carbon from soil to aquatic systems, the lateral transport of water, sediment and carbon can also affect the land carbon budget through several indirect ways. First, the lateral redistribution of surface runoff can affect the land carbon budget by altering soil wetness. Our simulation results reveal that the lateral redistribution of runoff can significantly change local soil wetness, especially in floodplains (Fig. ~~S10b~~S14b), where the increase in soil wetness can be larger than 10% (Fig. ~~S13b~~S17b). Soil wetness is a key controlling factor of plant photosynthesis (Knapp et al., 2001; Stocker et al., 2019; Xu et al., 2013). Benefiting from the increase in soil wetness, the NPP in many grid cells with a large area of floodplain has increased by more than 5% (Fig. 10b), although the NPP over the whole Europe only increased by 1% (Fig. 10). Changes in soil wetness can further alter soil temperature (Fig. ~~S13a~~S17a). As soil wetness and temperature are the two most important controlling factors of organic matter decomposition, the lateral redistribution of runoff can affect local land carbon budget by changing the Rh. Moreover, in ORCHIDEE-$C_{lateral}$, the turnover times of litter and SOC under flooding waters (assumed to experience anaerobic condition) are set to be ~~three times~~one third of the litter and SOC turnover times in upland soil (Reddy & Patrick Jr, 1975; Neckles & Neill, 1994; Lauerwald et al., 2017). Accounting for flooding thus decreases the decomposition rate of litter and SOC stored in floodplain soils.

Second, soil erosion and sediment deposition can affect land carbon budget by altering the vertical distribution of litter and soil organic carbon. At the net erosion sites of the uplands, the loss of surface soil results in a part of the belowground litter and SOC that were originally stored in deeper soil layers emerging to the surface soil layers, and also results in a fraction of the belowground litter becoming the aboveground litter. In the floodplains, the newly deposited sediment becomes part of the ~~new~~ surface soil layer, and the belowground litter and SOC in the original surface soil layer is transferred down to the deeper soil layers. As the temperatures and fresh organic matter inputs (sourced from the aboveground litterfall and dead roots), which can impact SOC decomposition rates through the priming effect (Guenet et al., 2016; Guenet et al., 2010), in different soil layers are different, changes in the vertical distribution of belowground litter and SOC can therefore lead to changes in the overall decomposition rate of the organic matter in the whole soil column.

Third, soil aggregates mostly break down during soil erosion and sediment transport, the riverine POC thus loses part of its physically protection from decomposition (Hu and Kuhn, 2016; Lal, 2003). Some modelling studies have assumed that at least 20% of the eroded SOC would be decomposed during the soil erosion and transport processes (Lal, 2003, 2004; Zhang et al., 2014). However, the estimation by Smith et al. (2001) using a conceptual mass balance model suggest that only a tiny fraction of the eroded POC is decomposed and released as CO_2 to the atmosphere. Using laboratory rainfall-simulation experiments, van Hemelryck et al. (2010) estimated a 2%-12% mineralization of the eroded SOC from a loess soil, and Wang et al. (2014) estimated a mineralization of only 1.5%. In ORCHIDEE-$C_{lateral}$, the passive SOC pool is regarded as the SOC associated to soil minerals and protected by soil aggregates. The turnover time of the passive POC in river stream and flooding waters is assumed to be same to that of the active POC (0.3 year). Our simulation results suggest that the fraction of total riverine POC that is decomposed during the lateral transport from uplands to the sea is 2.9% in Europe (Fig. ~~7b), and the~~7b), which is larger than the POC decomposition fraction (0.9%) when the turnover time of the passive POC in rivers is assumed to be same to that of the passive POC (i.e. no soil aggregates break down). The acceleration of POC decomposition rate due to the breakdown of soil aggregates can thus slightly affect the estimate of the regional land-atmosphere carbon flux. Moreover, the riverine POC and DOC can be transported over a long distance and finally settle or infiltrate in floodplains or river channels (especially the Estuarine deltas) where the local environmental conditions might be quite different from those encountered in the uplands from where these C pools originate. These changes in environmental conditions can affect the decomposition rate of the laterally redistributed organic carbon (Abril et al., 2002).

Comparison between the simulation results from ORCHIDEE-$C_{lateral}$ with activated and deactivated erosion and river routing modules indicate that ~~the~~ ignoring ~~of~~ lateral carbon transport processes in LSM may lead to significant biases in the simulated land carbon budget (Figs. 10 and ~~S11~~S15). Although the omission of lateral carbon transport in ORCHIDEE-$C_{lateral}$

only resulted in a 1% decrease in simulated average annual total NPP in Europe during 1901-2014 and a 1% increase of annual total Rh, the annual total NBP (=~~NPP–Rh~~NEP–Rd–DOC and POC to river) is ~~underestimated~~overestimated by 4.5%. Over the same period, the lateral carbon transport only induced a 0.09% ~~increase~~decrease in the total SOC and DOC stock in Europe (Fig. ~~S12c~~S16c), but their spatial distribution was significantly altered (Figs. 11e,f). For instance, in some mountainous regions, the soil erosion induced a reduction of the SOC stock by more than 8%. On the contrary, the sediment and POC deposition in some floodplains led to an increase in SOC stock by more than 8% (Fig. 11f).

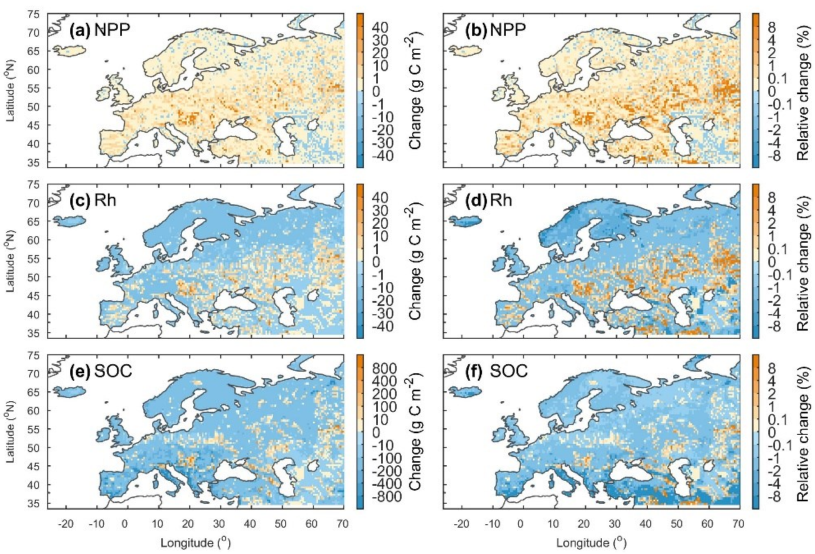

Figure 11 Changes (first column) and relative changes (second column) of the net primary production (NPP), heterotrophic respiration (Rh) and total soil organic carbon (SOC, 0-2 m) in Europe due to the lateral carbon transport during 1901-2014. For each variable, the change is calculated as $C_{lat} - C_{nolat}$, where C_{lat} and C_{nolat} are the carbon fluxes or stocks when lateral carbon transport is considered and ignored, respectively. The relative changes is calculated as $(C_{lat} - C_{nolat}) / C_{nolat} \times 100\%$.

Formatted: Font: 12 pt

Consistent with previous studies (Stallard, 1998; Smith et al., 2001; Hoffmann et al., 2013), our simulation results reveal the importance of sediment deposition in floodplains for the overall SOC budget. From 1901 to 2014, erosion and leaching over Europe totally induced a loss of 3.03 Pg organic carbon (POC+DOC) from uplands to the river network, and only 0.65 Pg of this carbon was redeposited onto the floodplains. The total stock of soil organic carbon in Europe thus should have decreased by 2.38 Pg C. However, due to the decrease in decomposition rate of the buried organic carbon (including in-situ and ex-situ carbon) in floodplain soils, the total stock of soil organic carbon in Europe only decreased by 0.91 Pg C. Floodplains in Europe have totally protected 2.12 (= 3.03 - 0.91) Pg soil organic carbon from been transported to the sea or be released to the atmosphere in forms of CO_2. Although the sequestration of organic carbon in floodplains cannot make up all of the soil organic carbon (POC+DOC) loss, the increased organic carbon stock in floodplains (2.12 Pg C) is much higher than the soil POC loss (0.86 Pg C) induced by soil erosion.

3.4 ~~Persisting short comings~~Uncertainties and future work

In the present version of ORCHIDEE-Clateral, the lateral transfers of sediment and carbon is simulated using a simplified scheme, due to the fragmented nature of large-scale forcing (e.g. geomorphic properties of the river channel) and validation data (e.g. continuous sediment and carbon concentration data in river streams and deposition/erosion rates in river channels). We recognize that this simplification induces significant uncertainties in model outputs, especially regarding changes in lateral sediment and particulate carbon transfers under climate change and direct human perturbations. Several physics-based algorithms have been proposed to accurately calculate the *TC* of stream flows (Arnold et al., 1995; Molinas and Wu, 2001; Nearing et al., 1989). These algorithms mostly require detailed information about the stream power (e.g. flow speed and depth), geomorphic properties of the river channel (e.g. slope and hydraulic radius) and the physical properties of the sediment particles (e.g. median grain size) (Neitsch et al., 2011). They are good predictors to estimate *TC* in rivers with detailed observation data on local stream, soil, geomorphic properties. Unfortunately, it is not practical to implement those algorithms in ORCHIDEE-$C_{lateral}$ due to the lack of appropriate forcing data at large scale as well as the relatively rough representation of stream flow dynamics compared to hydrological models for small basins. For example, runoff and sediment from all headwater basins in one 0.5° grid cell of ORCHIDEE-$C_{lateral}$ are assumed to flow into one single virtual river channel. Although the total river surface area in each grid cell is represented (obtained from forcing file (Table 1), Lauerwald et al., 2015), the length, width and depth of the river channel are unknown. Furthermore, in reality, there can be multiple river channels in the area represented by each grid cell, and these channels might flow to different directions.

We also noticed that previous studies have derived empirical functions of upstream drainage area (e.g. Luo et al., 2017) or upstream runoff (e.g. Yamazaki et al., 2011) to calculate the river width and depth, allowing to simulate the water flow in the river channel using physically-based algorithms. Unfortunately, to obtain a good fit of the simulated river discharges against observations, the parameters in the empirical functions for calculating river width and depth generally need to be calibrated separately for each catchment (Luo et al., 2017), an approach that is incompatible with large-scale simulations like those performed here. Without such calibration, the simulated geometrical properties of the river channel and runoff are prone to large uncertainties, thus rendering the simulation of sediment transport at continental or global scale using physically-based algorithms a more challenging task. Given the difficulty to simulate the detailed hydraulic dynamics of the stream flow at large spatial scale, we thus apply a simple approach described below to calculate the sediment transport capacity. Overall, we encourage future studies to produce large-scale databases on the geomorphic properties of global river channels (e.g. river depth and width) and to develop large-scale sediment transport models which can give a capable of producing more realistic and accurate simulations of sediment deposition, re-detachment and transport processes, as well as including the exchanges of water, sediment and carbon between river stream and floodplains.

The simulation of the soil DOC dynamics and leaching in our model need to be further improved to better simulate the seasonal variation of riverine DOC and TOC concentrations. The concentration of soil DOC and the DOC decomposition rate during the lateral transport process in the river network are the two key factors controlling DOC concentration in river flow. As only a small fraction (< 20%) of the riverine DOC is decomposed during lateral transport (Fig. 7), the overestimated (Fig. 5) seasonal amplitude in riverine DOC (and TOC) concentrations is likely caused by the uncertainties in the simulated seasonal dynamics of the leached soil DOC. The current scheme used in our model for simulating soil DOC dynamics has been calibrated against observed DOC concentrations at several sites in Europe (Camino-Serrano et al., 2018). Although the calibrated model can overall capture the average concentrations of soil DOC, it is not able to fully capture the temporal dynamics of DOC concentrations (Camino-Serrano et al., 2018). Given this, it is necessary to collect additional observation data on the seasonal dynamics of soil DOC concentration to further calibrate the soil DOC model. In addition, averaged over the various DOC and SOC pools we distinguish in the soils, DOC represents a much more reactive fraction of soil carbon (with a turnover time of several days to a few months) than SOC (with a turnover time of decades to thousands of years). Therefore, soil DOC concentrations experience large seasonal variations, while SOC concentrations generally are much more stable and show very limited seasonal dynamics. Overall, seasonal variations in riverine POC concentrations are mainly controlled by the seasonal dynamics of soil erosion rates, rather than by the seasonal SOC dynamics, which explains a partial decoupling in the behavior of POC compared to that of DOC.

Although most processes related to lateral carbon transport have been represented in ORCHIDEE-$C_{lateral}$, there are still omitted processes and large uncertainties in our model. For example, many studies suggest that a substantial portion of the eroded sediment and carbon is deposited downhill at adjacent lowlands as colluviums, rather than exported to the river (Berhe et al., 2007; Smith et al., 2001; Stallard, 1998Hoffmann et al., 2013; Wang et al., 2010). As the deposition of sediment and carbon within headwater basins can also significantly alter the vertical SOC profile and soil micro-environments (e.g. soil moisture, aeration and density) (Doetterl et al., 2016; Gregorich et al., 1998; Wang et al., 2015; Zhang et al., 2016), omission of this process may result in uncertainties in the simulated vegetation production and SOC decomposition. In addition, the impact of artificial dams and reservoirs on riverine sediment and carbon fluxes is also not represented in our model. Construction of dams generally leads to increased water residence time, nutrient retention, and sediment and carbon trapping in the impounded reservoir (Maavara et al., 2017), and can also affect the downstream flooding regime and frequency (Mei et al., 2016; Timpe and Kaplan, 2017). Estimation fromby Maavara et al. (2017) suggests that the organic carbon trapped or mineralized in global artificial reservoirs is about 13% of the total organic carbon carried by global rivers to the oceans. To more accurately simulate the lateral carbon transport, we plan to include the soil and carbon redistribution within headwater basins and the effects of dams and reservoirs on riverine sediment and carbon fluxes into our model in the near future.

The effects of lateral redistribution of water and sediment on vegetation productivity has not been fully represented in our model. As shown above, our model is able to represent the impacts of lateral water redistribution on vegetation productivity though modifying local soil wetness (Figs. 11 and ~~S13~~S17). However, in addition to modifying soil wetness, many studies have indicated that the soil erosion and sediment deposition can affect vegetation productivity by modifying soil nutrient (e.g. ~~e.g.~~ nitrogen (N) and phosphorus (P)) availability (Bakker et al., 2004; Borrelli et al., 2018; Quine, 2002; Quinton et al., 2010). Recently, terrestrial N and P cycles have already been incorporated into another branch of ORCHIDEE (i.e. the ORCHIDEE-CNP developed by Goll et al., 2017). By coupling our new branch and ORCHIDEE-CNP, it will be possible to develop a more comprehensive LSM that can also simulate the effects of lateral N and P redistribution on vegetation productivity.

~~Although soils are the major source of riverine organic carbon, domestic, agricultural and industrial wastes, as well as the river-borne phytoplankton can also make significant contributions (Abril et al., 2002; Meybeck, 1993). Moreover, previous studies have shown that sewage generally contains highly labile POC and most of the aquatic production can be mineralized within a short time (Abril et al., 2002; Caffrey et al., 1998). Omission of organic carbon inputs from manure, sewage and river-borne phytoplankton may be one of the main reasons for the underestimation of CO_2 evasion in the European river network, compared to the estimates using statistical models based on observed riverine DOC concentrations (Lauerwald et al., 2015; Raymond et al., 2013). Inclusion of these additional carbon sources should thus help reconcile simulated and observed riverine carbon concentrations and aquatic CO_2 evasion.~~

Although soils are the major source of riverine organic carbon, domestic, agricultural and industrial wastes, as well as river-borne phytoplankton can also make significant contributions (Abril et al., 2002; Meybeck, 1993; Hoffmann et al., 2020). Moreover, previous studies have shown that sewage generally contains highly labile POC while most of the aquatic production is generally mineralized within a short time (Abril et al., 2002; Caffrey et al., 1998). Omission of organic carbon inputs from manure and sewage could potentially lead to an underestimation of

CO_2 evasion from the European river network. Inclusion of these additional carbon sources should thus help improve simulation of aquatic CO_2 evasion.

Uncertainties in our simulation results also stem from the forcing data (Table 1) applied in our model. The routing scheme of water, sediment and carbon is driven by a map of stream flow direction at 0.5° spatial resolution (Guimberteau et al., 2012). Comparison between this flow direction map and the flow direction map derived based on high resolution (3″) DEM show discrepancies between the two river flow networks (Fig. ~~S5~~S7). As the flow direction directly determines the area of each catchment and the route of river flows, errors in forcing data of flow direction may thus induce uncertainties in the simulated riverine water, sediment and carbon discharges. Land-cover maps are another source of uncertainty. For instance, croplands generally experience significantly larger soil erosion rates than grasslands and forests (Borrelli et al., 2017; Nunes et al., 2011; Zhang et al., 2020). However, croplands in ORCHIDEE are only represented in a simplified way by segmenting them into C3 and C4 crops based on their photosynthesis characteristics. Therefore, our simulations based on land cover data with only two broad groups of crop might not be able to fully capture the seasonal dynamics of planting, canopy growth rate and harvesting for all crop types. Furthermore, the effects of soil conservation practices, which would decrease erosion rates, are ignored in our model. Panagos et al. (2015) have shown that contour farming, stone wall and grass margin techniques have been applied in Europe reduce the risk of soil erosion. However, these soil conservation practices only reduce the average erosion rate in European Union by 3%. Excluding soil conservation practices thus should have limited impact in our simulation results.

Further model calibration~~ and~~, evaluation~~, especially using~~ and development is necessary for improving our model. Due to the limitation of observation data~~ from regions outside of Europe, is necessary. In ORCHIDEE-C$_{lateral}$, an empirical equation (Eq. 8) adapted from the WBMsed model, which was originally proposed to simulate the total suspended sediment discharge in global rivers (Cohen et al., 2014), is used to estimate the transport capacities of clay, silt and sand sediment. By calibrating~~, we calibrated the parameters controlling sediment transport ~~capacity and the~~ , deposition ~~rate of excess suspended sediment (~~and re-detachment (i.e. ω, c_{rivdep}, c_{flddep}, c_{ebed} and c_{ebank} in Table ~~A1)~~ S1) in stream and flooding reservoirs only against the observed sediment ~~discharge rate in major European rivers (e.g. Rhine and Danube river),~~yield.

Even though our model can overall capture the sediment discharge rate in many European rivers (Fig. 3). Even so, there are still large uncertainties in the simulated sediment discharge rate (Fig. 3), and it islateral transfers of sediment and carbon in many rivers in central and northern Europe, more observation data are crucially needed to further evaluate the performance of our model, in particular in southern Europe. In addition, it is still unknown whether our model can satisfactorily simulate intermediate processes such as sediment deposition in river channels and floodplains, as well as the rate of river channel erosion. It is also unknown whether our model would perform satisfactorily in regions with very different climates than Europe (such as in the tropical regions).region. Thus, in the future, thean important aim iswill be to further calibrate our model against more detailed observation data (e.g. sediment deposition rate in river channels and floodplains) and extend the model applicationsapplication to contrasted regions or even the globe to refine the calibration of model parameters and evaluate its ability to on predict the lateral sediment and carbon transport across a wide range regions of contrasting climate regimes, vegetation and terrestrial biomestopography. Moreover, the GLORICH database (Hartmann et al., 2019)(Hartmann et al., 2019) only provides instantaneous observations of riverine organic carbon concentrations and it is therefore difficult to evaluate the model performance at annual or decadal scales.model's ability to reproduce temporal trends. Therefore, future modelling efforts should be combined with a data mining effortefforts targeting the collection of more continuous (e.g. daily) and long-term observational data of organic carbon content and fluxes in streams and rivers.

Conclusions

By merging ORCHILEAK (Lauerwald et al., 2017) and an upgraded version of ORCHIDEE-MUSLE (Zhang et al., 2020) for the simulation of DOC and POC from land to sea, respectively, we developed ORCHIDEE-$C_{lateral}$, a new branch of the ORCHIDEE LSM. ORCHIDEE-$C_{lateral}$ simulates the large-scale lateral transport of water, sediment, POC, DOC and CO_2 from uplands to the sea through river networks, the deposition of sediment and POC in river channels and floodplains, the decomposition POC and DOC during fluvial transport and the CO_2 evasion to the atmosphere, as well as the changes in soil wetness and vertical SOC profiles due to the lateral redistribution of water, sediment and carbon.

Evaluation using observation data from European rivers indicate that ORCHIDEE-$C_{lateral}$ can satisfactorily reproduce the observed riverine discharges of water and sediment, bankfull flows and organic carbon concentrations in river flows. Application of ORCHIDEE-$C_{lateral}$ to the entire European river network from 1901 to 2014 reveals that the average annual total carbon delivery to streams and rivers amounts to 47.3±6.6 Tg C yr^{-1}, which corresponds to about 4.7% of total NEP and 19.2% of the total NBP of terrestrial ecosystems in Europe. The lateral transfer of water, sediment and carbon can affect the land carbon dynamics through several different mechanisms. Besides directly inducing a spatial redistribution of organic carbon, it can also affect the regional land carbon budget by altering vertical SOC profiles, as well as the soil wetness and soil temperature, which in turn impact vegetation production and the decomposition of soil organic carbon. Overall, omission of lateral carbon transport in ORCHIDEE potentially results in an underestimation of the annual mean NBP in Europe of 4.5%. In regions experiencing high soil erosion or high sediment deposition rate, the lateral carbon transport also changes total SOC stock significantly, by more than 8%.

We recognize that ORCHIDEE-$C_{lateral}$ is still entailed with several limitations and significant uncertainties. To address those, we plan to enhance our model with additional processes, such as sediment deposition at downhills or the regulation of lateral transport by dams and reservoirs. We also plan to calibrate and evaluate further our model by extending the observational dataset to regions outside Europe.

Code and data availability

The source code of ORCHIDEE-Clateral model developed in this study is available online (https://doi.org/10.14768/f2f5df9f-26da-4618-b69c-911f17d7e2ed) from 22 July, 2019. All forcing and validation data used in this study are publicly available online. The specific sources for these data can be found in section Table 1.

Author contributions

HZ, RL and PR designed the study. HZ and RL conducted the model development and simulation experiments. PR, KV, PC, VN, BG and WY provided critical contribution to the model development and the design of simulation experiments. HZ conducted the model calibration, validation and the data analysis. RL, PR, PC, KV and BG provided support on collecting forcing and validation data. HZ, RL and PR wrote the manuscript. All authors contributed to interpretation and discussion of results and improved the manuscript.

Competing interests

The contact author has declared that neither they nor their co-authors have any competing interests.

Acknowledgements

HZ and PR acknowledges the ‘Lateral-CNP’ project (No. 34823748) supported by the Fonds de la Recherche Scientifique –FNRS and the VERIFY project that received funding from the European Union’s Horizon 2020 research and innovation program under grant agreement No. 776810. RL and PC acknowledge funding by the French state aid managed by the ANR under the "Investissements d'avenir" programme [ANR-16-CONV-0003_Cland]. P.R. received funding from the European Union’s Horizon 2020 research and innovation programme under Grant Agreement no. 101003536 (ESM2025 – Earth System Models for the Future).

1097

References:

Abotalib, A. Z., and Mohamed, R. S. A: Surface evidences supporting a probable new concept for the river systems evolution in Egypt: a remote sensing overview. Environ. Earth Sci., 69, 1621-1635, 2012.

Abrams, M., Crippen, R., and Fujisada, H.: ASTER Global Digital Elevation Model (GDEM) and ASTER Global Water Body Dataset (ASTWBD). Remote Sens., 12, 2020.

Abril, G., Nogueira, M., Etcheber, H., Cabecadas, G., Lemaire, E., and Brogueira, M. J.: Behaviour of organic carbon in nine contrasting European estuaries. Estuar., Coast. Shelf Sci., 54, 241-262, 2002.

Arnold, J. G., Williams, J. R., and Maidment, D. R.: Continuous-time water and sediment-routing model for large basins. J. Hydraul. Eng., 121, 171-179, 1995.

Bakker, M. M., Govers, G., and Rounsevell, M. D. A.: The crop productivity–erosion relationship: an analysis based on experimental work. Catena, 57, 55-76, 2004.

Battin, T. J., Luyssaert, S., Kaplan, L. A., Aufdenkampe, A. K., Richter, A., and Tranvik, L. J.: The boundless carbon cycle. Nat. Geosci.e, 2, 598-600, 2009.

Berhe, A. A., Harte, J., Harden, J. W., and Torn, M. S.: The Significance of the Erosion-induced Terrestrial Carbon Sink. BioScience, 57, 337-346, 2007.

Beusen, A. H. W., Dekkers, A. L. M., Bouwman, A. F., Ludwig, W., and Harrison, J.: Estimation of global river transport of sediments and associated particulate C, N, and P. Global Biogeochem. Cycles, 19, https://doi.org/10.1029/2005GB002453, 2005.

Borrelli, P., Robinson, D. A., Fleischer, L. R., Lugato, E., Ballabio, C., Alewell, C., Meusburger, K., Modugno, S., Schütt, B., Ferro, V., Bagarello, V., Oost, K. V., Montanarella, L., and Panagos, P.: An assessment of the global impact of 21st century land use change on soil erosion. Nat. Commun., 8, 2017.

Borrelli, P., Van Oost, K., Meusburger, K., Alewell, C., Lugato, E., and Panagos, P.: A step towards a holistic assessment of soil degradation in Europe: Coupling on-site erosion with sediment transfer and carbon fluxes. Environ. Res., 161, 291-298, 2018.

Caffrey, J. M., Coloern, J. E., and Grenz, C.: Changes in production and respiration during a spring phytoplankton bloom in San Francisco Bay, California, USA: implications for net ecosystem metabolism. Mar. Ecol. Prog. Ser., 172, 1-12, 1998.

Camino-Serrano, M., Guenet, B., Luyssaert, S., Ciais, P., Bastrikov, V., De Vos, B., Gielen, B., Gleixner, G., Jornet-Puig, A., Kaiser, K., Kothawala, D., Lauerwald, R., Peñuelas, J., Schrumpf, M., Vicca, S., Vuichard, N., Walmsley, D., and Janssens, I. A.: ORCHIDEE-SOM: modeling soil organic carbon (SOC) and dissolved organic carbon (DOC) dynamics along vertical soil profiles in Europe. Geosci. Model Dev., 11, 937-957, 2018.

Campoy, A., Ducharne, A., Cheruy, F., Hourdin, F., Polcher, J., and Dupont, J. C.: Response of land surface fluxes and precipitation to different soil bottom hydrological conditions in a general circulation model. J. Geophys. Res.: Atmos., 118, 10,725-710,739, 2013.

Castro, J. M., and Thorne, C. R.: The stream evolution triangle: Integrating geology, hydrology, and biology. River Res. Appl., 35, 315-326, 2019.

Chaplot, V. A. M., Rumpel, C., and Valentin, C.: Water erosion impact on soil and carbon redistributions within

Formatted: Space After: 0 pt

uplands of Mekong River. Global Biogeochem. Cycles, 19, GB4004, 2005.
Chappell, A., Baldock, J., and Sanderman, J.: The global significance of omitting soil erosion from soil organic carbon cycling schemes. Nat. Clim. Chang., 6, 187-191, 2016.
Chini, L. P., Hurtt, G. C., and Frolking, S.: Harmonized Global Land Use for Years 1500 – 2100, V1. Data set. Available on-line [http://daac.ornl.gov] from Oak Ridge National Laboratory Distributed Active Archive Center, Oak Ridge, Tennessee, USA, http://dx.doi.org/10.3334/ORNLDAAC/1248, 2014.
Ciais, P., Sabine, C., Bala, G., Bopp, L., Brovkin, V., Canadell, J., Chhabra, A., DeFries, R., Galloway, J., Heimann, M., Jones, C., Le Quéré, C., Myneni, R. B., Piao, S. L., and Thornton, P.: Carbon and Other Biogeochemical Cycles, in: Stocker, T. F., Qin, D., Plattner, G.-K., Tignor, M., Allen, S. K., Boschung, J., Nauels, A., Xia, Y., Bex, V., and Midgley, P. M. (Eds.), Climate Change 2013: The Physical Science Basis. Contribution of Working Group I to the Fifth Assessment Report of the Intergovernmental Panel on Climate Change Cambridge University Press, Cambridge, United Kingdom and New York, NY, USA, 2013.
Ciais, P., Yao, Y., Gasser, T., Baccini, A., Wang, Y., Lauerwald, R., Peng, S., Bastos, A., Li, W., Raymond, P. A., Canadell, J. G., Peters, G. P., Andres, R. J., Chang, J., Yue, C., Dolman, A. J., Haverd, V., Hartmann, J., Laruelle, G., Konings, A. G., King, A. W., Liu, Y., Luyssaert, S., Maignan, F., Patra, P. K., Peregon, A., Regnier, P., Pongratz, J., Poulter, B., Shvidenko, A., Valentini, R., Wang, R., Broquet, G., Yin, Y., Zscheischler, J., Guenet, B., Goll, D. S., Ballantyne, A. P., Yang, H., Qiu, C., and Zhu, D.: Empirical estimates of regional carbon budgets imply reduced global soil heterotrophic respiration. Natl. Sci. Rev., 8, https://doi.org/10.1093/nsr/nwaa145, 2021.
Cohen, S., Kettner, A. J., and Syvitski, J. P. M.: Global suspended sediment and water discharge dynamics between 1960 and 2010: Continental trends and intra-basin sensitivity. Glob. Planet. Change, 115, 44-58, 2014.
Cole, J. J., Prairie, Y. T., Caraco, N. F., McDowell, W. H., Tranvik, L. J., Striegl, R. G., Duarte, C. M., Kortelainen, P., Downing, J. A., Middelburg, J. J., and Melack, J.: Plumbing the Global Carbon Cycle: Integrating Inland Waters into the Terrestrial Carbon Budget. Ecosystems, 10, 172-185, 2007.
Coulthard, T. J., and Van de Wiel, M. J.: Modelling river history and evolution. Philosophical Transactions A Mathematical, Phys. Eng. Sci., 370, 2123-2142, 2012.
d'Orgeval, T., Polcher, J., and de Rosnay, P.: Sensitivity of the West African hydrological cycle in ORCHIDEE to infiltration processes, Hydrol. Earth Syst. Sci., 12, 1387–1401, https://doi.org/10.5194/hess-12-1387-2008, 2008.
Dirmeyerm, P. A., Gao, X., Zhao, M., Guo, Z., Oki, T., and Hanasaki, N.: GSWP-2: Multimodel Analysis and Implications for Our Perception of the Land Surface. Bull. Amer. Meteorol. Soc., 87, 1381-1398, 2006.
Doetterl, S., Berhe, A. A., Nadeu, E., Wang, Z., Sommer, M., and Fiener, P.: Erosion, deposition and soil carbon: A review of process-level controls, experimental tools and models to address C cycling in dynamic landscapes. Earth Sci. Rev., 154, 102-122, 2016.
Drake, T. W., Raymond, P. A., and Spencer, R. G. M.: Terrestrial carbon inputs to inland waters: A current synthesis of estimates and uncertainty. Limn.Oceanogr. Lett., 3, 132-142, 2018.
FAO/IIASA/ISRIC/ISSCAS/JRC: Harmonized World Soil Database (version 1.2), FAO, Rome, Italy and IIASA,

Laxenburg, Austria, 2012.

Galy, V., France-Lanord, C., and Lartiges, B.: Loading and fate of particulate organic carbon from the Himalaya to the Ganga–Brahmaputra delta. Geochim. Cosmochim. Acta, 72, 1767-1787, 2008.

Gassman, P. W., Sadeghi, A. M., and Srinivasan, R.: Applications of the SWAT Model Special Section: Overview and Insights. J. Environ. Qual., 43, 1-8, 2014.

Gregorich, E. G., Greer, K. J., Anderson, D. W., and Liang, B. C.: Carbon distribution and losses: erosion and deposition effects. Soil Tillage Res., 47, 291-302, 1998.

Guenet, B., Camino-Serrano, M., Ciais, P., Tifafi, M., Maignan, F., Soong, J. L., and Janssens, I. A.: Impact of priming on global soil carbon stocks. Glob. Change Biol., 24, 1873-1883, 2018.

Guenet, B., Moyano, F. E., Peylin, P., Ciais, P., and Janssens, I. A.: (2016) Towards a representation of priming on soil carbon decomposition in the global land biosphere model ORCHIDEE (version 1.9.5.2). Geosci. Model Dev., 9, 841-855, 2016.

Guenet, B., Neill, C., Bardoux, G., and Abbadie, L.: Is there a linear relationship between priming effect intensity and the amount of organic matter input? Appl. Soil Ecol., 46, 436-442, 2010.

Guimberteau, M., Drapeau, G., Ronchail, J., Sultan, B., Polcher, J., Martinez, J. M., Prigent, C., Guyot, J. L., Cochonneau, G., Espinoza, J. C., Filizola, N., Fraizy, P., Lavado, W., De Oliveira, E., Pombosa, R., Noriega, L., and Vauchel, P.: Discharge simulation in the sub-basins of the Amazon using ORCHIDEE forced by new datasets. Hydrol. Earth Syst. Sci., 16, 911-935, 2012.

Guimberteau, M., Zhu, D., Maignan, F., Huang, Y., Yue, C., Dantec-Nédélec, S., Ottlé, C., Jornet-Puig, A., Bastos, A., Laurent, P., Goll, D., Bowring, S., Chang, J., Guenet, B., Tifafi, M., Peng, S., Krinner, G., Ducharne, A., Wang, F., Wang, T., Wang, X., Wang, Y., Yin, Z., Lauerwald, R., Joetzjer, E., Qiu, C., Kim, H., and Ciais, P.: ORCHIDEE-MICT (revision 4126), a land surface model for the high-latitudes: model description and validation. Geosci. Model Dev., 11, 121-163, 2018.

Hanson, P. C., Hamilton, D. P., Stanley, E. H., Preston, N., Langman, O. C., and Kara, E. L.: Fate of allochthonous dissolved organic carbon in lakes: a quantitative approach. PLoS One, 6, e21884, 2011.

Haregeweyn, N., Poesen, J., Deckers, J., Nyssen, J., Haile, M., Govers, G., Verstraeten, G., and Moeyersons, J.: Sediment-bound nutrient export from micro-dam catchments in Northern Ethiopia. Land Degrad. Dev., 19, 136-152, 2008.

Hartmann, J., Lauerwald, R., and Moosdorf, N.: GLORICH - Global river chemistry database, in: PANGAEA (Ed.), 2019.

Hengl, T., de Jesus, J. M., MacMillan, R. A., Batjes, N. H., Heuvelink, G. B., Ribeiro, E., Samuel-Rosa, A., Kempen, B., Leenaars, J. G., Walsh, M. G., and Gonzalez, M. R.: SoilGrids1km--global soil information based on automated mapping. PLoS One, 9, e105992, 2014.

Hu, Y., Kuhn, N. J.: Erosion-induced exposure of SOC to mineralization in aggregated sediment. Catena, 137, 517-525, 2016.

Hoffmann, T. O.: 9.20 - Carbon Sequestration on Floodplains, in: Treatise on Geomorphology (Second Edition), edited by: Shroder, J. F., Academic Press, Cambridge, Massachusetts, United States, 10, 458-477, 2022,

https://doi.org/10.1016/B978-0-12-818234-5.00069-9.
Hoffmann, T. O., Baulig, Y., Fischer, H., and Blöthe, J.: Scale breaks of suspended sediment rating in large rivers in Germany induced by organic matter. Earth Surf. Dynam., 8, 661–678, 2020
Hoffmann, T., Schlummer, M., Notebaert B., Verstraeten, G., and Korup, O.: Carbon burial in soil sediments from Holocene agricultural erosion,Central Europe. Glob. Biogeochem. Cy., 27, 828-835, 2013.
Janssens, I. A., Freibauer, A., Ciais, P., Smith, P., Nabuurs, G. J., Folberth, G., Schlamadinger, B., Hutjes, R. W., Ceulemans, R., Schulze, E. D., Valentini, R., and Dolman, A. J.: Europe's terrestrial biosphere absorbs 7 to 12% of European anthropogenic CO2 emissions. Science, 300, 1538-1542, 2003.
Jetten, V., Govers, G., Hessel, R.: Erosion models: quality of spatial predictions. Hydrol. Process., 17, 887-900, 2003.
Kalbitz, K., Schmerwitz, J., Schwesig, D., and Matzner, E.: Biodegradation of soil-derived dissolved organic matter as related to its properties. Geoderma, 113, 273-291, 2003.
Knapp, A. K., Briggs, J. M., and Koelliker, J. K.: Frequency and Extent of Water Limitation to Primary Production in a Mesic Temperate Grassland. Ecosystems, 4, 19-28, 2001.
Krinner, G., Viovy, N., de Noblet-Ducoudré, N., Ogée, J., Polcher, J., Friedlingstein, P., Ciais, P., Sitch, S., and Prentice, I. C.: A dynamic global vegetation model for studies of the coupled atmosphere-biosphere system. Global Biogeochem. Cycles, 19, 2005.
Lal, R.: Soil erosion and the global carbon budget. Environ. Int., 29, 437-450, 2003.
Lal, R.: Soil carbon sequestration impacts on global climate change and food security. Science, 304, 1623-1627, 2004.
Lauerwald, R., Laruelle, G., Hartmann, J., Ciais, P., and Regnier, P.: Spatial patterns in CO_2 evasion from the global river network: Spatial patter of riverine pCO2 and FCO2. Global Biogeochem. Cycles, 29, 2015.
Lauerwald, R., Regnier, P., Camino-Serrano, M., Guenet, B., Guimberteau, M., Ducharne, A., Polcher, J., and Ciais, P.: ORCHILEAK (revision 3875): a new model branch to simulate carbon transfers along the terrestrial–aquatic continuum of the Amazon basin. Geosci. Model Dev., 10, 3821-3859, 2017.
Lauerwald, R., Regnier, P., Guenet, B., Friedlingstein, P., and Ciais, P.: How Simulations of the Land Carbon Sink Are Biased by Ignoring Fluvial Carbon Transfers: A Case Study for the Amazon Basin. One Earth, 3, 226-236, 2020.
Lehner, B., Verdin, K., and Jarvis, A.: New global hydrography derived from spaceborne elevation data. Eos, Transactions, AGU, 89, 93-94, 2008.
Lugato, E., Paustian, K., Panagos, P., Jones, A., and Borrelli, P.: Quantifying the erosion effect on current carbon budget of European agricultural soils at high spatial resolution. Glob. Change Biol., 22, 1976-1984, 2016.
Luo, X., Li, H., Leung L.R., Tesfa, T. K., Getirana, A., Papa, F., and Hess L. L.: Modeling surface water dynamics in the Amazon Basin using MOSART-Inundation v1.0: impacts of geomorphological parameters and river flow representation. Geosci. Model Dev., 10, 1233-1259, 2017.
Maavara, T., Lauerwald, R., Regnier, P., and Van Cappellen, P.: Global perturbation of organic carbon cycling by river damming. Nat. Commun., 8, 15347, 2017.

Formatted: Space After: 0 pt

Mei, X., Van Gelder, P., Dai, Z., and Tang, Z.: Impact of dams on flood occurrence of selected rivers in the United States. Front. Earth Sci., 11, 268-282, 2016.

Meybeck, M.: Riverine transport of atmospheric carbon: sources, global typology and budget. Water Air Soil Pollut., 70, 443-463, 1993.

Molinas, A., and Wu, B.: Transport of sediment in large sand-bed rivers. J. Hydraul. Res., 39, 135-146, 2001.

Moore, I. D., and Wilson, J. P.: Length-slope factors for the Revised Universal Soil Loss Equation: Simplified method of estimation. J. Soil Water Conserv., 47, 423-428, 1992.

Nadeu, E., de Vente, J., Martínez-Mena, M., and Boix-Fayos, C.: Exploring particle size distribution and organic carbon pools mobilized by different erosion processes at the catchment scale. J. Soils Sediments, 11, 667-678, 2011.

Naipal, V., Lauerwald, R., Ciais, P., Guenet, B., and Wang, Y.: CE-DYNAM (v1): a spatially explicit process-based carbon erosion scheme for use in Earth system models. Geosci. Model Dev., 13, 1201-1222, 2020.

Nakhavali, M., Lauerwald, R., Regnier, P., Guenet, B., Chadburn, S., and Friedlingstein, P.: Leaching of dissolved organic carbon from mineral soils plays a significant role in the terrestrial carbon balance. Glob. Change Biol., 27, 1083-1096, 2021.

Nardi, F., Annis, A., Di Baldassarre, G., Vivoni, E.R., and Grimaldi, S.: GFPLAIN250m, a global high-resolution dataset of Earth's floodplains. Sci. Data, 6, 180309, 2019.

Nearing, M. A., Foster, G. R., Lane, L. J., and Finkner, S. C.: A Process-Based Soil Erosion Model for USDA-Water Erosion Prediction Project Technology. Transactions of the Asae, 32, 1587-1593, 1989.

Neckles, H. A, and Neill, C.: Hydrologic control of litter decomposition in seasonally flooded prairie marshes. Hydrobiologia, 286, 155-165, 1994.

Neitsch, S. L., Williams, J. R., Arnold, J. G., and Kiniry, J. R.: Soil and Water Assessment Tool Theoretical Documentation Version 2009. Texas Water Resources Institute, College Station, 2011.

Nie, X., Li, Z., He, J., Huang, J., Zhang, Y., Huang, B., Ma, W., Lu, Y., and Zeng, G.: Enrichment of organic carbon in sediment under field simulated rainfall experiments. Environ. Earth Sci., 74, 5417-5425, 2015.

Nodvin, S. C., Driscoll, C. T., and Likens, G. E.: Simple partitioning of anions and dissolved organic carbon in a forest soil. Soil Sci., 142, 27-35, 1986.

Nunes, A. N., de Almeida, A. C., and Coelho, C. O. A.: (2011) Impacts of land use and cover type on runoff and soil erosion in a marginal area of Portugal. Appl. Geogr., 31, 687-699, 2011.

Oeurng, C., Sauvage, S., and Sánchez-Pérez, J. M.: Assessment of hydrology, sediment and particulate organic carbon yield in a large agricultural catchment using the SWAT model. J. Hydrol., 401, 145-153, 2011.

Parton, W. J., Schimel, D. S., Cole, C. V., and Ojima, D. S.: Analysis of Factors Controlling Soil Organic Matter Levels in Great Plains Grasslands1. Soil Sci. Soc. Am. J., 51, 1173-1179, 1987.

Parton, W. J., Stewart, J. W. B., and Cole, C. V.: Dynamics of C, N, P and S in grassland soils: a model. Biogeochemistry, 5, 109-131, 1988.

Polyakov, V. O., and Lal, R.: Soil organic matter and CO 2 emission as affected by water erosion on field runoff plots. Geoderma, 143, 216-222, 2008.

Quine, T. A.: An investigation of spatial variation in soil erosion, soil properties and crop production with an agricultural field in Devon, UK. J. Soil Water Conserv., 57, 55-65, 2002.

Quinton, J. N., Govers, G., Van Oost, K., and Bardgett, R. D.: The impact of agricultural soil erosion on biogeochemical cycling. Nat. Geosci., 3, 311-314, 2010.

Raymond, P. A., Hartmann, J., Lauerwald, R., Sobek, S., McDonald, C., Hoover, M., Butman, D., Striegl, R., Mayorga, E., Humborg, C., Kortelainen, P., Durr, H., Meybeck, M., Ciais, P., and Guth, P.: Global carbon dioxide emissions from inland waters. Nature, 503, 355-359, 2013.

Reddy, K. R., Patrick Jr, and W. H.: Effect of alternate aerobic and anaerobic conditions on redox potential, organic matter decomposition and nitrogen loss in a flooded soil. Soil Biol. Biochem., 7, 87-94, 1975.

Regnier, P., Friedlingstein, P., Ciais, P., Mackenzie, F. T., Gruber, N., Janssens, I. A., Laruelle, G. G., Lauerwald, R., Luyssaert, S., Andersson, A. J., Arndt, S., Arnosti, C., Borges, A. V., Dale, A. W., Gallego-Sala, A., Goddéris, Y., Goossens, N., Hartmann, J., Heinze, C., Ilyina, T., Joos, F., LaRowe, D. E., Leifeld, J., Meysman, F. J. R., Munhoven, G., Raymond, P. A., Spahni, R., Suntharalingam, P., and Thullner, M.: Anthropogenic perturbation of the carbon fluxes from land to ocean. Nat. Geosci., 6, 597-607, 2013.

Reynolds, C., Jackson, T., and Rawls, W.: Estimating available water content by linking the FAO soil map of the world with global soil profile databases and pedo-transfer functions, Am. Geophys. Union Fall Meet. EOS Trans. Spring Meet. Suppl., 80, S132, 1999.

Sanderman, J., Hengl, T., and Fiske, G. J.: Soil carbon debt of 12,000 years of human land use. Proc. Natl. Acad. Sci., 114, 9575-9580, 2017.

Schneider, C., Flörke, M., Eisner, E., and Voss, F.: Large scale modelling of bankfull flow: An example for Europe. J. Hydrol., 408, 235-245, 2011.

Shangguan, W., Dai, Y., Duan, Q., Liu, B., and Yuan, H.: A global soil data set for earth system modeling. J. Adv. Model. Earth Syst., 6, 249-263, 2014.

Sharpley, A. N., and Williams, J. R.: EPIC-erosion/productivity impact calculator: 2. User manual. Technical Bulletin - United States Department of Agriculture, 4, 206-207, 1990.

Smith, S. V., Renwick, W. H., Buddemeier, R. W., and Crossland, C.J.: Budgets of soil erosion and deposition for sediments and sedimentary organic carbon across the conterminous United States. Global Biogeochem. Cycles, 15, 697-707, 2001.

Stallard, R. F.: Terrestrial sedimentation and the carbon cycle: Coupling weathering and erosion to carbon burial. Global Biogeochem. Cycles, 12, 231-257, 1998.

Stocker, B. D., Zscheischler, J., Keenan, T. F., Prentice, I. C., Seneviratne, S. I., and Peñuelas, J.: Drought impacts on terrestrial primary production underestimated by satellite monitoring. Nat. Geosci., 12, 264-270, 2019.

Telmer, K., and Veizer, J.: Carbon fluxes, pCO_2 and substrate weathering in a large northern river basin, Canada: carbon isotope perspectives. Chem. Geol., 159, 61-86, 1999.

Tian, H., Yang, Q., Najjar, R. G., Ren, W., Friedrichs, M. A. M., Hopkinson, C. S., and Pan, S.: Anthropogenic and climatic influences on carbon fluxes from eastern North America to the Atlantic Ocean: A process-based modeling study. J. Geophys. Res.: Biogeosci., 120, 757-772, 2015.

Timpe, K., and Kaplan, D.: The changing hydrology of a dammed Amazon. Sci. Adv., 3, 11, e1700611, 2017.

Van Hemelryck, H., Govers, G., Van Oost, K., and Merckx, R.: Evaluating the impact of soil redistribution on the in situ mineralization of soil organic carbon. Earth Surf. Process. Landf., 36, 427-438, 2011.

Van Oost, K., Quine, T. A., Govers, G., De Gryze, S., Six, J., Harden, J. W., Ritchie, J. C., McCarty, G. W., Heckrath, G., Kosmas, C., Giraldez, J. V., da Silva, J. R., and Merckx, R.: The impact of agricultural soil erosion on the global carbon cycle. Science, 318, 626-629, 2007.

Vigiak, O., Malago, A., Bouraoui, F., Vanmaercke, M., Obreja, F., Poesen, J., Habersack, H., Feher, J., and Groselj, S.: Modelling sediment fluxes in the Danube River Basin with SWAT. Sci. Total Environ., 599-600, 992-1012, 2017.

Vörösmarty, C. J., Fekete, B. M., Meybeck, M., and Lammers, R. B.: Geomorphometric attributesof the global system of rivers at 30-minute spatial resolution. J. Hydrol., 237, 17-39, 2000.

Wang, X., Cammeraat, E. L., Romeijn, P., and Kalbitz, K.: Soil organic carbon redistribution by water erosion--the role of CO2 emissions for the carbon budget. PLoS One, 9, e96299, 2014a.

Wang, Z., Govers, G., Steegen, A., Clymans, W., Van den Putte, A., Langhans, C., Merckx, R., and Van Oost, K.: Catchment-scale carbon redistribution and delivery by water erosion in an intensively cultivated area. Geomorphology, 124, 65-74, 2010.

Wang, Z., Hoffmann, T., Six, J., Kaplan, J. O., Govers, G., Doetterl, S., and Van Oost, K.: Human-induced erosion has offset one-third of carbon emissions from land cover change. Nat. Clim. Chang., 7, 345-349, 2017.

Wang, Z., Van Oost, K., and Govers, G.: Predicting the long-term fate of buried organic carbon in colluvial soils. Global Biogeochem. Cycles, 29, 65-79, 2015.

Wang, Z., Van Oost, K., Lang, A., Quine, T., Clymans, W., Merckx, R., Notebaert, B., and Govers, G.: The fate of buried organic carbon in colluvial soils: a long-term perspective. Biogeosciences, 11, 873-883, 2014b.

Xu, X., Sherry, R. A., Niu, S., Li, D., and Luo, Y.: Net primary productivity and rain-use efficiency as affected by warming, altered precipitation, and clipping in a mixed-grass prairie. Glob. Change Biol., 19, 2753-2764, 2013.

Yamazaki, D., Kanae, S., Kim, H., and Oki T.: A physically based description of floodplain inundation dynamics in a global river routing model. Water Resour. Res., 47, W04501, doi:10.1029/2010WR009726, 2011.

Zhang, H., Lauerwald, R., Regnier, P., Ciais, P., Yuan, W., Naipal, V., Guenet, B., Van Oost, K., and Camino-Serrano, M.: Simulating Erosion-Induced Soil and Carbon Delivery From Uplands to Rivers in a Global Land Surface Model. J. Adv. Model. Earth Syst., 12, e2020MS002121, 2020.

Zhang, H., Liu, S., Yuan, W., Dong, W., Xia, J., Cao, Y., and Jia, Y.: Loess Plateau check dams can potentially sequester eroded soil organic carbon. J. Geophys. Res. Biogeosci., 121, 2016.

Zhang, H., Liu, S., Yuan, W., Dong, W., Ye, A., Xie, X., Chen, Y., Liu, D., Cai, W., and Mao, Y.: Inclusion of soil carbon lateral movement alters terrestrial carbon budget in China. Sci. Rep., 4, 7247, 2014.